



Influence of material modeling on warm forming behavior of nickel based super alloy

Anand Badrish¹ · Ayush Morchhale¹ · Nitin Kotkunde¹ · Swadesh Kumar Singh²

Received: 12 November 2019 / Accepted: 17 February 2020 / Published online: 27 February 2020
© Springer-Verlag France SAS, part of Springer Nature 2020

Abstract

The present study helps in providing a systematic approach towards the investigation of deep drawing and stretch forming processes for Inconel 625 alloy. Firstly, the flow stress nature and material properties of Inconel 625 super-alloy have been investigated and it has been found that temperature and deformation rate significantly affects the flow stress behavior. By using experimental flow stress data, four different constitutive models namely; modified Johnson-Cook (m-JC), modified Zerilli-Armstrong (m-ZA), modified Arrhenius (m-A), Khan–Huang–Liang (KHL) model have been formulated of which m-A has been found to have the best predictability for flow stress. Hill 1948 and Barlat 1989 anisotropic yield criterion have also been applied and it has been found that Barlat 1989 criteria more accurately capture the yielding behavior of Inconel 625 alloy. The deep drawing analysis has been carried out using target and noise performance measures for different process parameters viz., temperature, punch speed and blank holding pressure. Uniformity in thickness has been major cause of concern, hence experiment at 473 K, 5 mm/min speed and 20 Bar pressure was found to have least variation in thickness. Furthermore, the forming limit diagram (FLD) and fracture curve (FC) obtained from stretch forming analysis along five different strain paths was found to be significantly affected by temperature. Further, user defined material (UMAT) subroutine have been incorporated in ABAQUS 6.13 software to have effect of m-A model and Barlat 1989 yield criteria in finite element analysis (FEA) of deep drawing and stretch forming processes.

Keywords Inconel 625 alloy · Constitutive model · Yield criteria · Deep drawing · Stretch forming · Finite element analysis

Nomenclature

σ	Flow Stress
ϵ	Plastic Strain
$\dot{\epsilon}$	Deformation rate
A	Yield Stress
B	Strain-hardening coefficient
m	Thermal softening exponent
n	Strain hardening exponent
T_m	Melting temperature of Inconel 625 (1609 K)
T	Testing temperature
T_{ref}	Reference temperature (298 K)
R	Universal gas constant

Q	Activation Energy
A'	Structural factor
α	Stress multiplier
n_1	Stress exponent
C	Strain rate hardening coefficient
D_p^0	Random upper bound strain rate at 300 K (10^6 s^{-1})
K	Strength coefficient
U	Ultimate Strength
%El	Elongation percentage
$\dot{\epsilon}_{ref}$	Reference deformation rate (0.01 s^{-1})

Introduction

Inconel 625 is a nickel-chromium based super alloy. Its demand is increasing continuously in nuclear, petrochemical, marine, aerospace and automotive industries as it is having extraordinary mechanical properties and capability of withstanding extreme environmental conditions. In addition, it is also having good weldability and is resistant towards creep,

✉ Nitin Kotkunde
nitink@hyderabad.bits-pilani.ac.in

¹ Mechanical Engineering Department, BITS-Pilani, Hyderabad, Telangana, India

² Mechanical Engineering Department, GRIET, Hyderabad, India

thermal shock and aqueous corrosion [1]. Inconel 625 possess limited workability at room temperature (RT) as it is having very complex microstructure with high strength and resistance towards deformation. Moreover, it is difficult to machine due to the presence of hard abrasive carbide, work hardening characteristics and extreme toughness even at elevated temperature [2].

Rigorous efforts, financial support, huge amount of time and availability of material are required for carrying out any of experimental procedure. Therefore, theoretical constitutive models are used for predicting the flow stress behavior. Several statistical parameters are used to compare the accuracy of used constitutive models. Few studies have been done in past specifically for Nickel based alloys in order to establish the constitutive relations from experimental data to elaborate the complex hot deformation behavior for process parameters such as strain, strain rates and temperature effects [3–5]. Grzesik et al. [6] used Johnson Cook model for the prediction of Flow stress behavior of Inconel 718 alloy and further validated the numerically predicted flow stress with the experimentally obtained one. Gujrati et al. [7] applied several constitutive model, namely, Sellars model also known as modified Arrhenius model, Schöck-Seeger-Wolf model and Kocks model to predict the best flow stress behavior for solution treated Inconel 718 alloy and found that Sellar model has the best prediction capability at all the considered test temperatures and strain rates in uniaxial compression test. Wen et al. [4] investigated Nickel based superalloys for a range of 980–1040 °C temperature with 0.01 and 0.1 s⁻¹ as strain rates with the help of processing maps. Lin et al. [3] tested nickel based alloys for 920–1040 °C temperature and 0.001–1 s⁻¹ strain rate with the help of hot compression test and found that flow stress decreased with increase in deformation temperature and decrease in strain rate. In order to explain the dynamic flow softening, dynamic recovery and strain hardening behavior of Ni-based superalloys, studies were conducted in past with the help of phenomenological constitutive models [8, 9]. Effect of δ -phase and hard abrasive carbides over mechanical properties at high temperature (650–700 °C) for Inconel 625 have been studied by Liu et al. [10]. The increased size of δ -phase due to solution treatment resulted in overall decrement in elongation at fracture of metal. A constitutive relation has been proposed by Lin et al. [5] for defining the deformation behavior of Inconel alloy at 0.001–0.1 s⁻¹ strain rate and 920–1040 °C temperature. Considering the visco-plastic constitutive relation for dynamic recovery behavior and work hardening of a material, this newly developed model has good predictability ($R > 0.9925$), avg. absolute relative error (4.06%) at a lower temperature but is unable to estimate the stress flow behavior at higher strain-rates and temperatures because of complete dislocation of δ -phase (Ni₃Nb) at these conditions. Work hardening performance of Ni-based aged super alloys at the time of hot deformation has been influenced

by deformation temperature, presence of δ phases, strain and strain rates.

Yield criteria are the one used for predicting the yield behavior of any material when it undergoes deformation. Yield criteria consist of two types isotropic and anisotropic for respective type of metals. Hill 1948 and Barlat 1989 are some of the most popular yield criteria because they are easy in understanding and predicts very good yielding behavior for a large number of constants. Yield criteria are very much useful in case when numerical analysis is used for prediction of deformation behavior of material [11]. Prasad et al. [12] in his previous work over IN718 alloy used Barlat 1989 yield criteria for prediction of Forming Limit Diagram by Numerical analysis approach. Kotkunde et al. [13] in his work over Experimental and numerical investigation of anisotropic yield criteria for warm deep drawing of Ti–6Al–4 V alloy used different yield criteria from Hill and Barlat yield criteria family and concluded that the Cazacu Barlat criterion is best suited for the numerical analysis of deep drawing process and also concluded that combination of yield criteria with constitutive model is very much important for the accurate prediction of deformation behavior in any material forming processes.

Sheet metal forming plays a very important role in automotive, aerospace and nuclear industries [14]. Forming process such as deep drawing [1] and stretch forming [15] depends upon a large number of process parameters and their interdependence upon each other. The main process parameters which influences the formability are working temperature, punch speed, blank holding pressure, lubricant, sheet thickness and dimensions of die and punch [1, 16–19]. In industry, extensive trial and error method is carried out to arrive the optimum set of process parameters. This process is very tedious and time-consuming to arrive an optimum setting and quality product. Thus, the experiments need to be designed in such a way that optimization of selected process parameters can be done in a way to reduce manufacturing cost and improve the quality of product. Effect of various parameters on deep drawing of AA7075 was investigated and finally the results were supported by finite element analysis (FEA) by Venkateswarlu et al. [20]. He found temperature to be the most significant parameter for effective deep drawing of AA7075. The effective control over a blank holding force improved the final quality of a product for AA 2008-T4 alloy as reported by Ahmetoglu et al. [21]. Wallmeier et al. [22] reported that some of the mechanical properties such as hardening exponent, yield stress and elastic modulus also play a major role in deep thickness distribution and forming load in deep drawing process. Prasad et al. [23] reported that punch force and friction between die, blank and blank holder plate helps in deciding the overall thinning rate during deep drawing process. Analysis of variance (ANOVA) is a collection of statistical models and their associated estimation procedures (such as the “variation” among and between groups) used to analyze the differences

among group means in an obtained experimental sample values. The ANOVA is based on the law of total variance, where the observed variance in a particular variable is partitioned into components attributable to different sources of variation. The reason for using ANOVA is to identify the parameters that significantly influence the quality characteristic. The concept of ANOVA and Analysis of means (ANOM) have been applied by Padmanabhan et al. [24] to understand the effect of individual process parameter over deep drawability of mild steel. Choudhary et al. [25] optimized 11 different process parameter settings with the help of ANOVA and Signal to Noise (S/N) ratio analysis for Al 1100 and Al 6061 alloys in V bending process for minimizing the springback effect as it plays a very important role in the forming of metals. Badrish et al. [26] also used Taguchi analysis in optimizing the process parameters for minimizing the springback of IN625 alloy.

Forming limit diagram (FLD) represents the surface strain limits which a sheet metal can withstand under severe loading conditions with substantially less amount of localized necking. FLD is segregated into two different loading paths viz., Tensile-Compressive (T-C) and Tensile-Tensile (T-T) [12]. Various procedures have been suggested by researchers in past to plot FLD by following separate loading paths along which a material can undergo plastic deformation for aluminum [27, 28], stainless steel [29, 30], titanium [13, 31] and automotive grade low carbon steels [32, 33]. By following proper parameters of tool designing and process selection for metal forming, manufacturing industries can increase production by many folds. FEA software can also be used for prediction of FLD with high precision [12, 23]. Prasad et al. [23] investigated the FLD of solution treated or processed Inconel 718 alloy and found strain at fracture of specimen along different strain paths in T-T and T-C zones. He further evaluated forming ability of material on the basis of thickness distribution, surface strain plot and Limit drawing height (LDH). Roamer et al. [34] compared FLD of Inconel 625LCF, 718 and 718SPF alloys at room temperature condition and found that all three alloys show similar nature only in T-C zone. He also found that second phase particles increased in alloy 718

due to which its FLD shifted to lower major strain as compared to others.

Recently, fracture forming limit diagram (FFLD) has been used by many researchers for predicting the failure of sheet materials in which fracture/tearing has been observed without a substantially visible necking. In order to plot FFLD, the fracture strain is required to be measured in the thickness direction and the surface fracture strains need to be estimated considering failure under a plane strain deformation mode [35–39]. There has been no open literature available on FFLD for IN625 material, and hence, in general view has been shared over FFLD. The evaluation of FFLD was of immense interest in incremental sheet metal forming processes [37] where the failure is always in the form of splitting/tearing without the onset of prior necking. It has been reported that the FFLDs of aluminum and steel sheets have linear shape showing higher ductility limit, and the shape was well characterized as per ductile failure criteria [39]. Embury and Duncan [38] first reported similar kind of observations in equi-biaxial tensile deformation of Al alloys (6061 and 2036-T4), where the formability limits by necking and fracture interacted in such a way that the fracture of the sheet took place without prior localized necking. The shape and failure limit strains of automotive grade sheets depend on the type of failure mode resulting from the void nucleation, growth and coalescence from the presence of inclusions, precipitates, hard second-phase particles, etc., and also from the activation of shearing instabilities.

On the basis of extensive literature survey, it has been observed that considerable research is available with traditional metallic alloys of steel, titanium and aluminum etc. at different testing conditions. However, very spare efforts were made in past to understand the formability behavior of high strength super alloys such as Inconel 625 alloy. Thus, an effort is made in present study for predicting the flow stress behavior of Inconel 625 alloy using various phenomenological and physical constitutive models. Deep drawing experiments have been performed in order to find the forming ability of Inconel 625 with varying process parameters viz., temperature (T), punch speed (PS) and blank holding pressure (BHP). Stretch forming

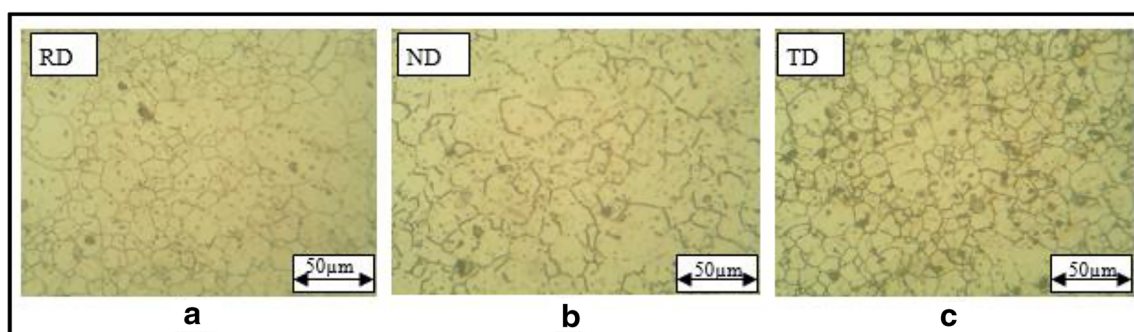
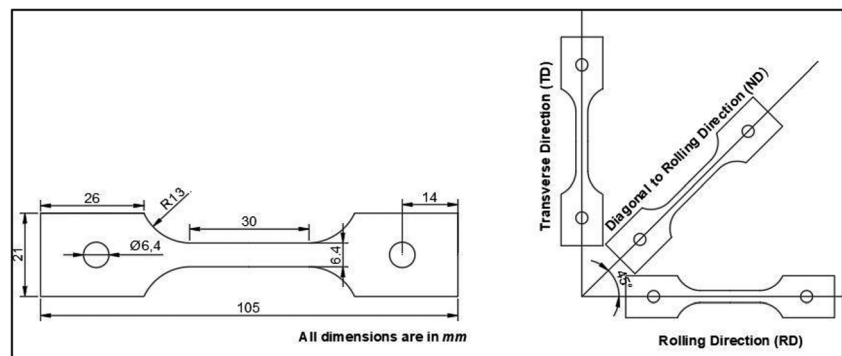


Fig. 1 Microstructure of as-received Inconel 625 alloy sheet (a) RD (b) ND (c) TD

Fig. 2 Schematic representation of tensile test specimen with three different orientations



was also performed to see the effect of temperature over forming limit and further full FLD has been plotted for Inconel 625 alloy. Additionally, FEA study of deep drawing and stretch forming process have been conducted by having using best combination of constitutive model with yield criteria using user defined material code (UMAT) in ABAQUS 6.13 software and the obtained FEA results were validated with the experimental one.

Materials and methods

Inconel 625 superalloy sheet of 1 mm thickness has been used for all the experiments in present work. It is an alloy having major contribution of Nickel (61.49%), Chromium (21.73%) and Molybdenum (9.47%) elements which helps in providing it strength and ductility. It also contain other elements such as Niobium (3.27%) and Aluminum (0.067%) which are

responsible for age hardening as a result of $\text{Ni}_3(\text{Al}, \text{Nb})$ precipitates which exist as ellipsoidal γ' phase homogeneously over whole metallic sheet and restrains creep at elevated testing temperatures [40]. It also contain other elements such as Titanium (0.166%), Manganese (0.123%) and Iron (Balance). The initial microstructure of as received Inconel 625 alloy sheet with respect to different orientations (RD, ND and TD) have been shown in Fig. 1. The optical microscope has been used for observing the microstructure. Average ASTM number for grain size was 9. Mechanical properties observed in RD at various temperatures have been better than at the other two directions (TD and ND) because the grains were fine and elongated in RD.

ASTM E08/E8M-11 standard [41] has been referred for preparing tensile test specimen. For considering the anisotropic effect, the tensile test samples were prepared by considering 3 different orientations with respect to grains orientation namely, 0° or RD, 45° or ND and 90° or TD as shown in Fig. 2. Tensile testing of samples have been performed with deformation rate (0.01 , 0.001 and 0.0001 s^{-1}) and temperature (300 K, 473 K and 673 K). Each set of experiment has been repeated 3 times and average values are reported for discussion.

Deep drawing and stretch forming process have been performed over hydraulic press equipped with induction type setup for high temperature experiments. Contact type thermocouple (K-type) has been used during entire experimentation to have an accurate observation over temperature. The deep drawing experiments have been performed at various temperature (300 K, 473 K and 673 K), blank holding pressure (15, 20 and 25 Bar) and punch speed (1, 5 and 10 mm/min). Blanks of 58 mm diameter are used for deep drawing in present work. Stretch forming has been performed at different temperature (300 K, 473 K and 673 K) with fixed BHP of 25 Bar and 5 mm/min speed. Circular grid of 3 mm diameter was marked over stretch forming specimens using laser etching process for strains in different regions. Each set of experiment has been repeated 3 times and average values are reported for discussion. The schematic diagram of deep drawing and stretch forming setup with five different designs of specimens are shown in Figs. 3 and 4 respectively. Rectangle shaped specimens have been used by many researchers for stretch forming

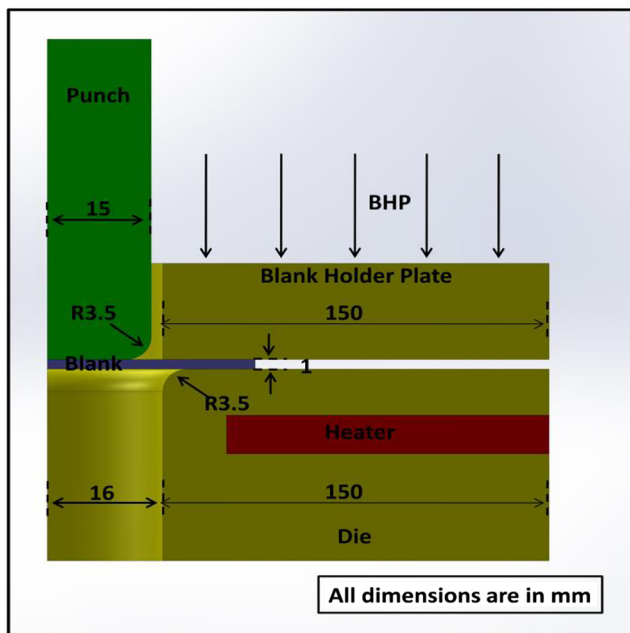


Fig. 3 Schematic representation of deep drawing setup

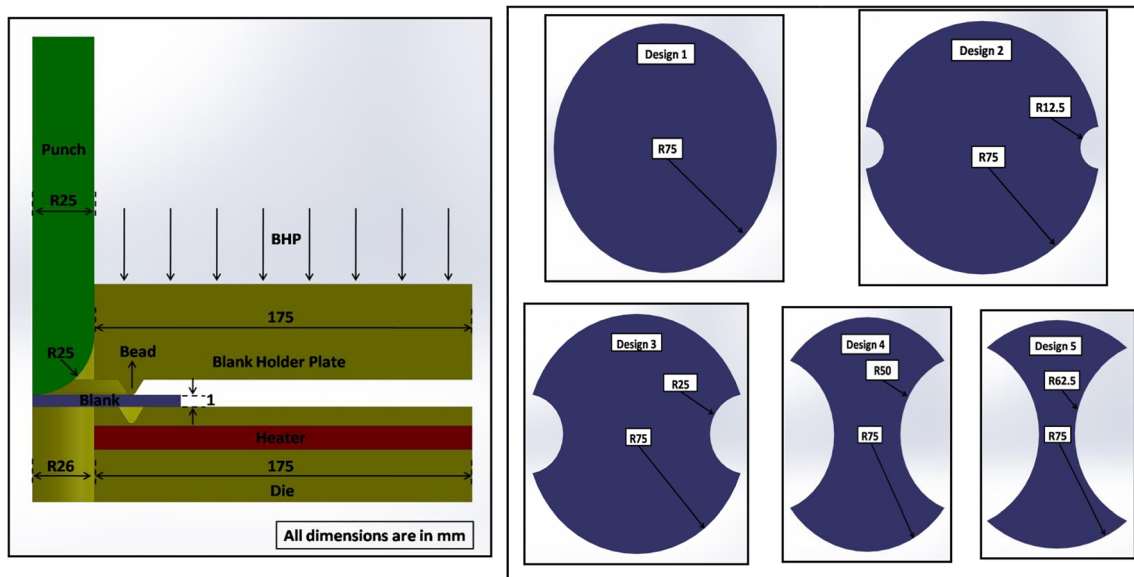


Fig. 4 Schematic representation of stretching setup with 5 different types of specimens

analysis but these specimens fail easily from the draw bead as the width of specimen decreases, hence, hasek specimen have been mentioned in ASTM E2218–15 standard to be used for successfully determining the limiting strains of material. The stereo microscope with a image analyzing software has been used for measuring the major and minor strain over the deformed surface. In the present work, a sub-sized hemispherical punch of $\phi 50$ mm has been used instead of the standard punch of $\phi 101.4$ mm as proposed by Hecker [42]. Figure 5 shows the induction setup used in deep drawing and stretching process.

Results and discussion

Material properties and deformation behavior

The representative plot for true stress-strain with respect to varying temperature, deformation rate and specimen orientation are shown in Fig. 6 (a), (b) and (c) respectively. The flow stress seems to decrease with increase in temperature. Usually

with increase in deformation rate, the flow also increases but no such particular trend was observed in present case. The flow stress seems to decrease with increase in angle of sheet in reference to RD as the grains get elongated more in rolling direction which results in higher strength before failure. Initially steep increase in stress have been observed in comparison to strain for all the specimens till yielding point has been achieved because of macroscopic deformations which majorly occur due to initial movement of dislocations. This is followed by slow increase till ultimate strength and finally sudden failure of specimen occur [43].

The material properties of Inconel 625 alloy at different deformation rate and temperature with orientation as RD are displayed in Fig. 7. Yield and ultimate strength of material are found to be highly dependent upon temperature as they decreased by an amount of approximately 25% and 17% respectively as temperature increased to 673 K from 300 K. Dislocation density is an important factor required for defining the yielding strength of any material. Mechanism of dislocation comprises of three steps viz., its generation, gliding

Fig. 5 Induction setup used in (a) Deep drawing and (b) Stretching process

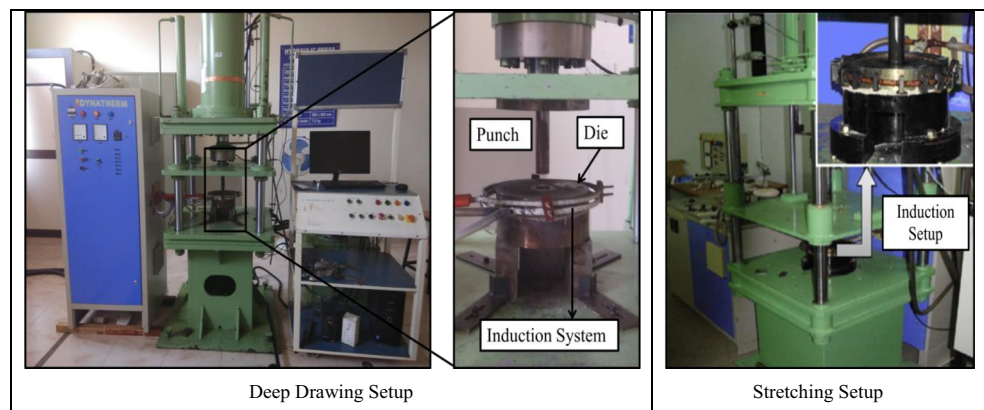


Fig. 6 Representative true stress-strain plot for varying (a) temperature, (b) deformation rate and (c) orientation

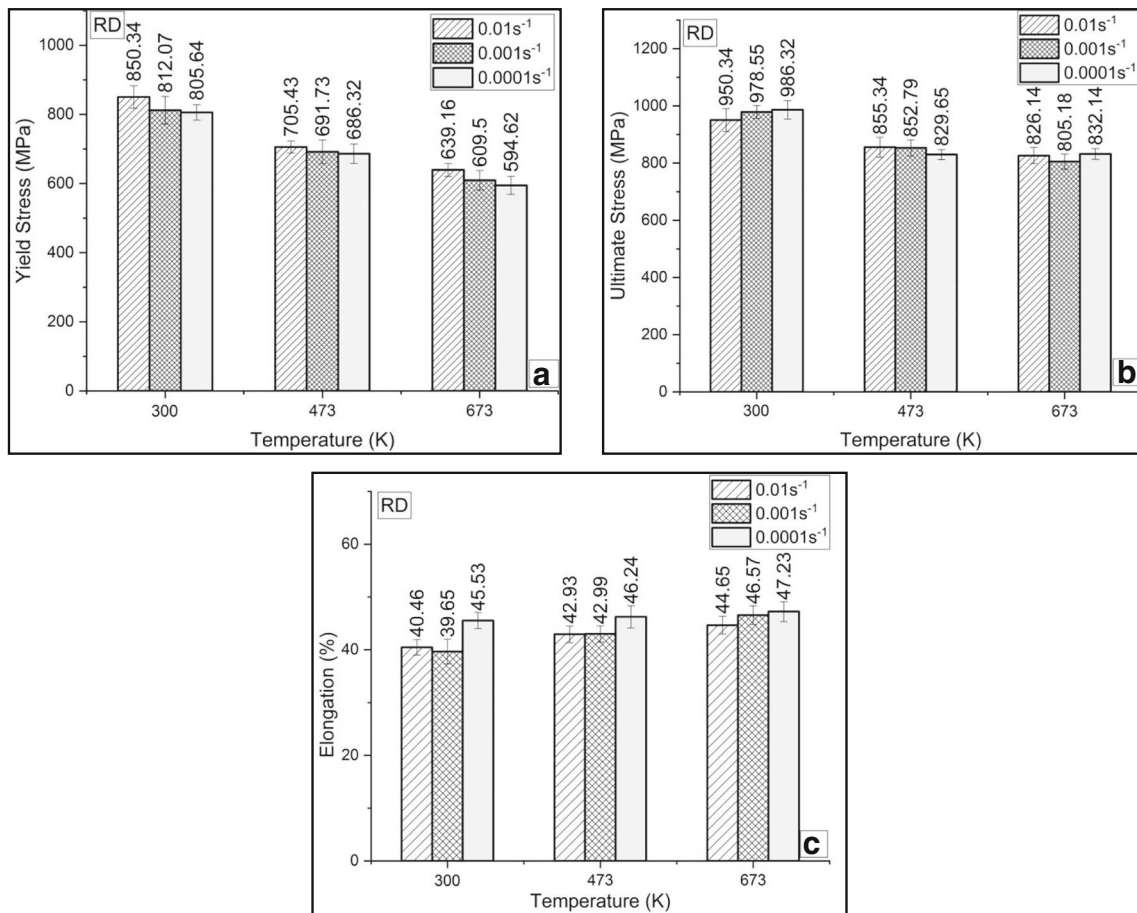
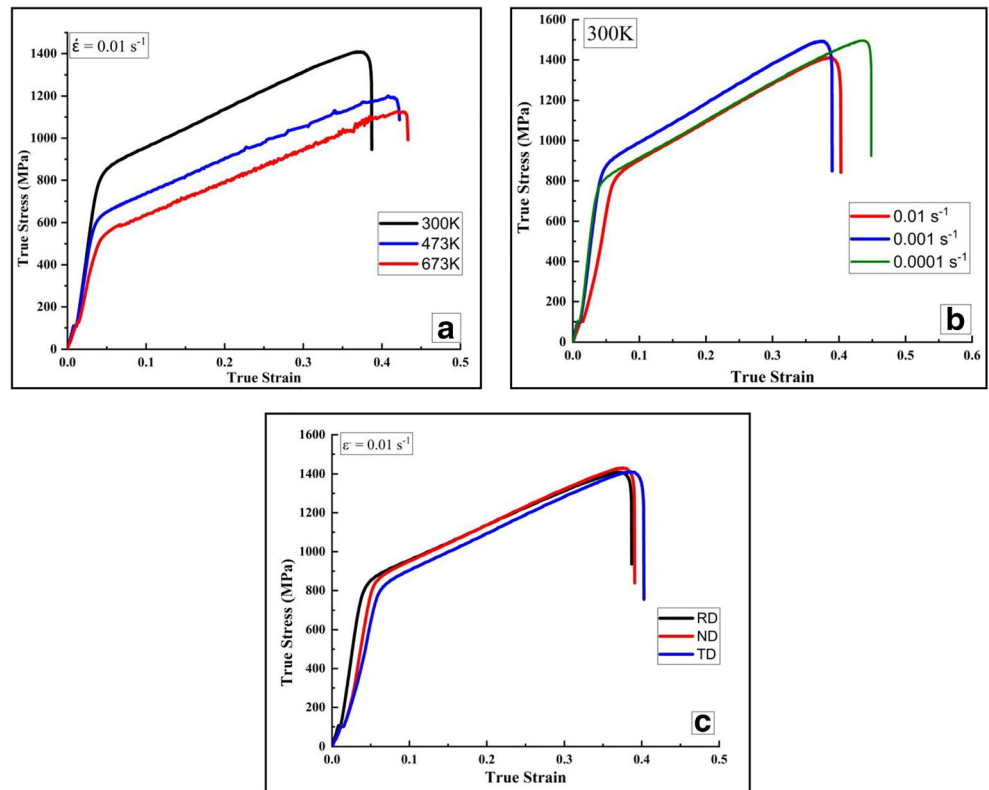
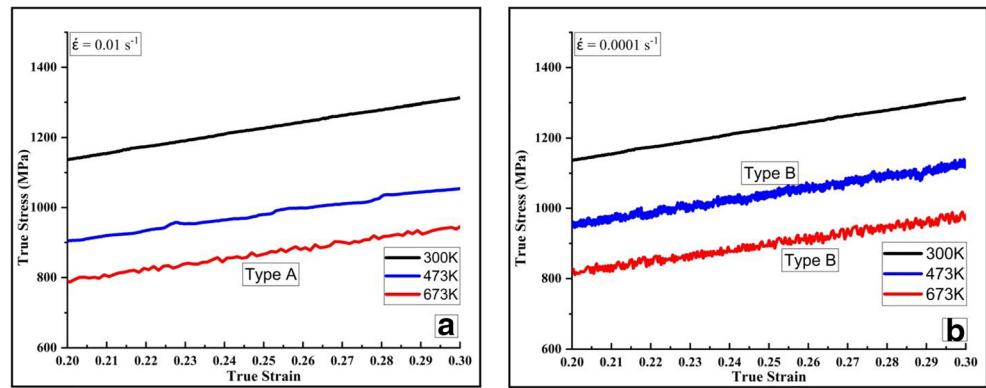


Fig. 7 Material properties (a) Yield Strength, (b) Ultimate Strength and (c) % Elongation for Inconel 625 alloy

Fig. 8 Serrated nature of flow stress plots at (a) 0.01 s^{-1} and (b) 0.0001 s^{-1}



and annihilation. Plastic deformation majorly occur due to these dislocations. At lower temperatures, activation energy required for movement of atoms is high which results in creating hindrance for easy movement of dislocations. As a result, metal shows high strength at room temperature. Dislocation mechanisms can be delayed by work hardening. With increase in atomic level vibrations at elevated temperature, the internal energy also increases which in turn helps in decreasing the hindrances for movement of dislocations. Easy climbing or gliding of dislocation and finally annihilation of dislocations results in compression and expansion of metallic structure at higher temperature which results in reduction of its overall strength as compared to room temperature. But, easy gliding of grain boundaries at higher temperature help in improving the ductility of material [44, 45].

Serrated nature of flow stress has been observed at higher temperature for Inconel 625 alloy as shown in Fig. 8(a) and (b) for orientation as RD and deformation rate as 0.01 and 0.0001 s^{-1} respectively. The serrated behavior of flow stress increased with decrease in deformation rate. A process in which nucleation and growth of grains takes place at the time of ongoing deformation and not afterwards as a different process i.e. a process ends randomly before starting of successive process is known as dynamic recrystallization (DRX). Rapid DRX is the reason of such serrated nature of graph [46]. Serration for metals are classified into type A, B and C by Rodriguez [47]. No serrations are observed at 300 K for Inconel 625 alloy in the present case. Type B serrations are observed at 473 K only at 0.0001 s^{-1} deformation rate. At 673 K, type A and type B serrations are observed for 0.01 s^{-1} and 0.0001 s^{-1} deformation rate respectively. Lin

et al. [48] also made similar observations about serrated nature of flow stress for the Inconel alloy.

Dynamic Strain Ageing (DSA) effect can also be used for explaining such serrated nature of flow stress curves. DSA effect can be confirmed by negative strain rate sensitivity (m) [49]. ‘ m ’ is numerically calculated by Eq. 1. The DSA effect can also be stated as the strengthening mechanism which can be related as the solid solution strengthening for a variety of fcc and bcc substitutional and interstitial alloys. The variation of flow stress behavior with respect to the change in strain rate is generally calculated based on strain rate sensitivity ‘ m ’ value. Generally, the ‘ m ’ value is measured experimentally by comparing the stress levels, at the same strain of two tensile tests at different strain rate for a particular testing temperature. Table 1 represents the ‘ m ’ calculated at different temperature and sheet orientations. ‘ m ’ value is observed to be positive for 300 K which indicates no serration. At 673 K, negative ‘ m ’ value is observed at all the sheet orientations which confirms the DSA effect and hence serrated nature of flow stress curve. The DSA phenomenon occurs due to the segregation of dislocations from solute atoms at lower strain rates [50]. This in turn decreases the energy, which results in easy dislocation movements when compared with solute-free dislocations. At lower temperatures and higher strain rates, the movement of dislocations is faster than the diffusion of solute atoms into the dislocations. Thus, the drag force minimize as the dislocations are solute-free. The flow gets localized in a narrow region due to negative strain rate sensitivity, which propagates along the specimen as Luder’s lines [51]. At higher temperatures, the value of ‘ m ’ is higher due to the increased rate of thermally activated processes, such as grain boundary sliding and dislocation climb [52].

Table 1 Strain rate sensitivity (m) at different temperature and orientations

Orientation	300 K	473 K	673 K
RD	0.0064	0.0035	-0.0017
ND	0.0018	0.0042	-0.0062
TD	0.0026	-0.0004	-0.0038

Table 2 Material constants for m-JC constitutive model

A_1 (MPa)	B_1 (MPa)	B_2 (MPa)	C_1	λ_1	λ_2
695.06	1486.2	-681.3	0.0081	-0.0003	0.0026

Table 3 Material constants for m-ZA model

A(MPa)	B(MPa)	C ₃	C ₄	C ₅	C ₆	n
850	1213.7	5.317×10 ⁻⁴	-6.816×10 ⁻⁴	-0.0072	9.44×10 ⁻⁵	0.3012

$$m = \frac{\dot{\epsilon} \, d\sigma}{\sigma \, d\dot{\epsilon}} = \left(\frac{\partial(\ln\sigma)}{\partial(\ln\dot{\epsilon})} \right)_{\epsilon, T} \quad (1)$$

Material modeling

Constitutive modeling

Various phenomenological models viz., modified Jhonson-Cook (m-JC) [53], Khan–Huang–Liang (KHL) [54], modified Arrhenius (m-A) [55] and physical models viz., modified Zerilli-Armstrong (m-ZA) [56] have been applied for determining flow stress behavior of Inconel 625 alloy in present work.

Modified Jhonson-Cook (m-JC) model

Deformation rate, temperature and strain are some of the process parameters used in defining original JC model [53]. It is a phenomenological flow stress model. Relation defining original JC model is shown below in Eq. 2.

$$\sigma = (A + B\epsilon^n) \left(1 + C \ln \frac{\dot{\epsilon}}{\dot{\epsilon}_{ref}} \right) \left(1 - \left(\frac{T - T_{ref}}{T_m - T_{ref}} \right)^m \right) \quad (2)$$

Material constants A, B and n varied with testing temperature. JC model helps in predicting independent effects of process parameters over flow stress but it fails to define the coupled effects of deformation rate and temperature [57]. Thus, modification have been proposed and m-JC equation is shown below in Eq. 3.

$$\sigma = (A_1 + B_1\epsilon + B_2\epsilon^2) \left(1 + C_1 \ln \frac{\dot{\epsilon}}{\dot{\epsilon}_{ref}} \right) \exp \left[\left(\lambda_1 + \lambda_2 \ln \frac{\dot{\epsilon}}{\dot{\epsilon}_{ref}} \right) (T - T_{ref}) \right] \quad (3)$$

where, A₁, B₁, B₂, C₁, λ₁, λ₂ are material constants of m-JC model. The calculation of material constants shown below in Table 2 can be done by following procedure defined according to Lin et al. [58].

Table 4 Material constants for m-A constitutive model

α(MPa ⁻¹)	n'	Q (kJ/mol)	A'(s ⁻¹)
0.00097	63.885	104.0925	1.4010

Modified Zerilli-Armstrong (m-ZA) model

Theory of dislocation mechanism which has major role in defining the flow stress of material in presence of critical loading circumstances, helps in defining the relation given by Zerilli Armstrong [56]. Many important modifications have been suggested and implemented in original relation. The m-ZA relation is defined below in Eq. 4.

$$\sigma = (A + B\epsilon^n) \exp \left\{ (-C_3 + C_4\epsilon)(T - T_{ref}) \right\} + \left[C_5 + C_6(T - T_{ref}) \ln \left(\frac{\dot{\epsilon}}{\dot{\epsilon}_{ref}} \right) \right] \quad (4)$$

where, C₃, C₄, C₅ and C₆ are different material constants calculated according to Samantaray et al. [59] and are shown below in Table 3.

Modified Arrhenius (m-A) model

This model helps in establishing a relation between testing temperature, deformation rate and flow stress. m-A equation [9, 55] uses Zener-Hollomon (Z) term as defined below in Eq. 5, which is an exponential relation representing coupled effect of temperature and deformation rate over flow stress.

$$Z = \dot{\epsilon} \exp \left(\frac{Q}{RT} \right) \quad (5)$$

The Arrhenius constitutive relation is defined as shown below in Eq. 6. All the constant of m-A equation are calculated according to previous work done by Kotkunde et al. [1]. Table 4 shows the values of material constants calculated for m-A relation.

$$\dot{\epsilon} = A' \left[\sinh(\alpha\sigma) \right]^{n'} \exp \left(-\frac{Q}{RT} \right) \quad (6)$$

Khan–Huang–Liang (KHL) model

KHL model [53] is used in finding the predicted flow stress and it is expressed using Eq. 7. This model helps

Table 5 Material constants for KHL model

A(GPa)	B ₁ (GPa)	n ₀	n ₁	C'	m'
0.8494	1.213	0.1670	1.2530	0.0101	0.0584

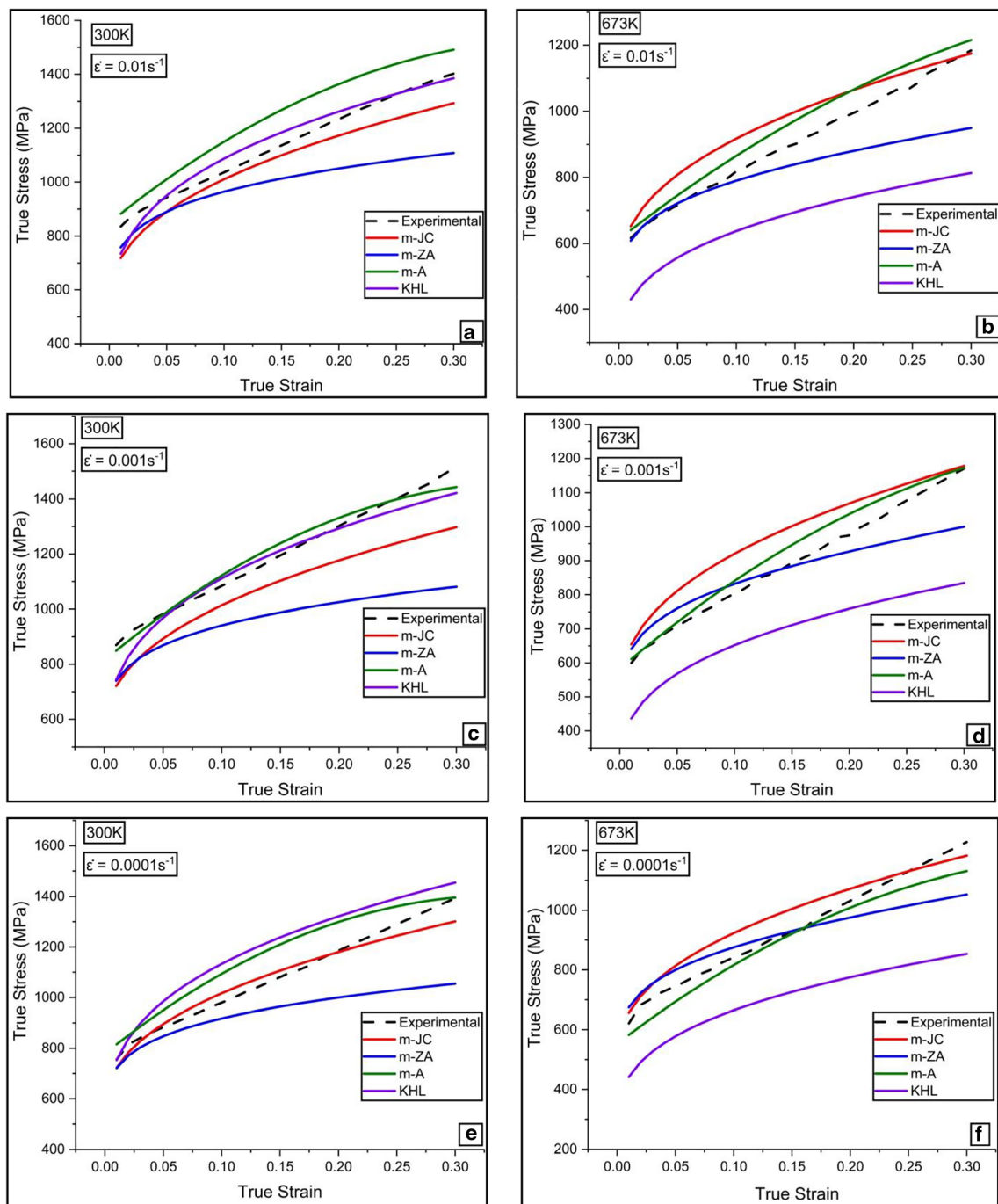


Fig. 9 Predicted and experimental flow stress at different testing parameters

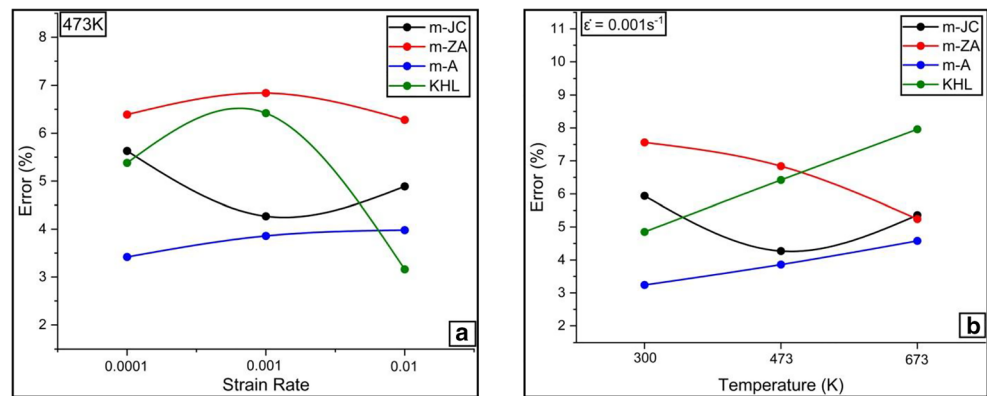
Table 6 Statistical parameters compared for different constitutive models

	m-JC	m-ZA	KHL	m-A
R	0.9326	0.9265	0.9122	0.9721
Δ (%)	6.6142	6.9561	7.2534	5.2616
δ (%)	5.5260	6.2862	6.9267	2.3140

in defining the complex path of loading for deformation of material. All the constants viz., A, B₁, C', n₀, n₁ and m' are calculated according to the steps followed by Prasad et al. [60]. The calculated material constants are mentioned in Table 5.

$$\sigma = \left[A + B \left(1 - \frac{\ln \varepsilon}{D_p^0} \right)^{n_1} \varepsilon^{n_0} \right] \left(\frac{\varepsilon}{\varepsilon_{ref}} \right)^{c'} \left(\frac{T_m - T}{T_m - T_{ref}} \right)^{m'} \quad (7)$$

Fig. 10 Representative variation of Error (%) with (a) temperature and (b) deformation rate



The applicability of considered constitutive models are compared using various statistical parameters viz., average absolute relative error (Δ), standard deviation (δ) and correlation coefficient (R) in present work for Inconel 625 alloy. Figure 9 shows representative predicted flow stress curves at different deformation rates and temperatures. $\Delta\%$ and $\delta\%$ are used for analyzing the prediction accuracy of models as R is considered to be biased parameter toward upper or lower limits of whole flow stress domain [61]. Table 6 shows the comparison of different statistical parameters for Inconel 625 alloy. m-JC, KHL and m-ZA models have comparable results but still $\Delta\%$ and $\delta\%$ values are considered to be on higher side. Among all these models, m-A model shows best prediction capability with highest R and lowest $\Delta\%$ and $\delta\%$ values. Thus, modified-Arrhenius model is in very good agreement with experimental flow stress data for Inconel 625 alloy.

The constitutive models are applied for FEA of forming studies at elevated temperature and hence it is very important to consider the sensitivity effect of deformation rate and temperature [9]. Therefore, error in predicted results at various deformation rate and temperature have been observed for different considered constitutive models. Figure 10(a) and (b) shows representative plot for error percent in predictability of flow stress. Error percent is found on higher side for all the models except m-A for Inconel 625 alloy. Error percent is least deviated throughout the testing range in case of m-A for both deformation rate and temperature. The m-A model also considers the combined effect of deformation rate, activation energy and temperature while predicting the flow stress which other models fail to do so. Hence, m-A model is considered during FEA of deep drawing process for Inconel 625 alloy in present work.

Table 7 Constants calculated for Hill 1948 criterion

Temperature	H	G	F	N
300 K	0.614015	0.540103	0.459897	1.694937
473 K	0.325208	0.547765	0.452235	1.180086
673 K	0.739487	0.47918	0.52082	1.415115

Anisotropic yield criterion

Sheet metals shows difference in mechanical properties along different directions because of rolling process characteristics and their respective crystallographic structure. This is known as anisotropic behavior of metal [1, 62]. Anisotropy is majorly induced due to rolling process and it is characterized by 3 different orthogonal planes. Barlat 1989 and Hill 1948 are two criteria considered in present study for determining the anisotropic yielding behavior of Inconel 625 alloy.

Hill 1948 yield criterion

Hill [63] in 1948 proposed a coupled effect of planar anisotropy with yield function given by von-Mises. Yielding response of material can be shown in terms of constitutive relation in elasto-plastic region having combined plastic hardening and yield stress effect in it. Eq.8 shows the extended version of yield function proposed by Hill.

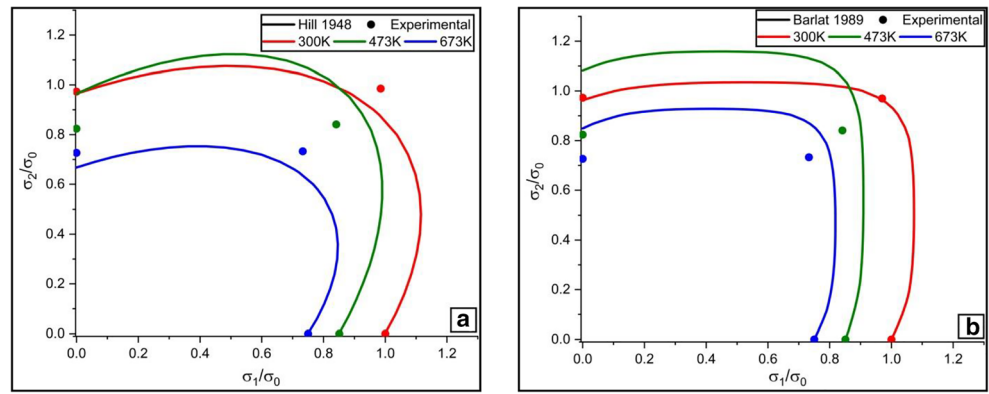
$$f(\sigma) = \tilde{\sigma}^2 = F\sigma_{yy}^2 + G\sigma_{xx}^2 + H(\sigma_{xx} - \sigma_{yy})^2 + 2N\sigma_{xy}^2 \quad (8)$$

where, N , H , G and F are anisotropic material coefficients. σ_{xx} , σ_{yy} and σ_{xy} are stress along defined directions in subscripts. On the basis of σ -value and r -value method, the calculation of these material constants can be done but r -value approach is used in present study. All the constants have been evaluated from the procedure followed by Banabic [64] and are shown in Table 7.

Table 8 Constants calculated for Barlat 1989 criterion

Temperature	a	c	h	p
300 K	0.887581	1.112419	1.036294	0.89
473 K	0.845991	1.154009	0.785926	0.67
673 K	1.025793	0.974207	0.881727	0.94

Fig. 11 Yielding behavior of Inconel 625 alloy with (a) Hill 1948 and (b) Barlat 1989 criterion



Barlat 1989 yield criterion

Yield function having planar stress effect was developed by Barlat [65]. It is displayed by Eq.8.

$$2\tilde{\sigma}^m = a|k_1 + k_2|^m + a|k_1 - k_2|^m + c|2k_2|^m = \phi \tag{9}$$

where, k_2 and k_1 are terms that can be expressed as.

$$k_1 = \frac{\sigma_1 - h\sigma_2}{2} \tag{10}$$

$$k_2 = \sqrt{\left(\frac{\sigma_1 - h\sigma_2}{2}\right)^2 - p^2\tau_{12}^2} \tag{11}$$

In Eq. 9–11, h , a and c are anisotropy ratio functions. These can be formulated as.

$$a = 2\left(1 - \sqrt{\frac{r_0 r_{90}}{(1+r_0)(1+r_{90})}}\right) \tag{12}$$

$$h = \sqrt{\frac{r_0(1+r_{90})}{r_{90}(1+r_0)}} \tag{13}$$

$$c = (2-a) \tag{14}$$

Here, r_{90} and r_0 are TD and RD direction anisotropic ratio of sheet metal. p value as used in Eq. 15 is calculated iteratively [65]. Lankford parameter variation with angle from rolling direction is considered for calculation of p value. It is expressed in Eq.15.

$$R = \frac{2m\sigma_0^m}{\sigma_\theta \left(\frac{\partial\phi}{\partial\sigma_{11}} + \frac{\partial\phi}{\partial\sigma_{22}}\right)} - 1 \tag{15}$$

Here, θ is considered to be 45° . In Eq.8 and 14, m is a parameter dependent on crystallography of material and is

Table 9 Average thickness obtained for different set of process parameters

Experiment No.	Temperature, T (K)	BHP (bar)	Punch speed, PS (mm/min)	Average Experimental Thickness (mm)	S/N ratio
1	300	15	1	0.913	32.8930
2	300	15	5	0.931	39.3716
3	300	15	10	0.942	35.7061
4	300	20	1	0.976	40.1255
5	300	20	5	0.928	47.4582
6	300	20	10	0.937	37.1139
7	300	25	1	0.928	34.8149
8	300	25	5	0.919	36.3699
9	300	25	10	0.937	30.2910
10	473	15	1	0.929	43.5962
11	473	15	5	0.899	32.9783
12	473	15	10	0.903	36.7837
13	473	20	1	0.906	35.0400
14	473	20	5	0.929	48.6884
15	473	20	10	0.919	34.9924
16	473	25	1	0.907	48.0656
17	473	25	5	0.900	40.2850
18	473	25	10	0.924	41.6086
19	673	15	1	0.939	33.0476
20	673	15	5	0.903	42.8996
21	673	15	10	0.917	32.8873
22	673	20	1	0.916	28.9168
23	673	20	5	0.957	45.9013
24	673	20	10	0.937	43.2571
25	673	25	1	0.927	37.3801
26	673	25	5	0.934	33.7171
27	673	25	10	0.927	35.5911

Table 10 ANOVA for TPM (mean thickness distribution)

Source	DF	Seq. SS	F-Value	P Value	% Contribution
Temperature	2	0.001674	6.03	0.009	49.80
BHP	2	0.000956	3.44	0.052	28.44
Punch Speed	2	0.000359	0.21	0.810	10.68
Residual Error	20	0.000372	–	–	11.06
Total	26	0.003361	–	–	100

called as exponent of yield function ($m = 8$ in present case). All the constants have been calculated according to the procedure followed by Banabic [64] and are shown in Table 8.

The yield loci comparison for Hill 1948 and Barlat 1989 with experimental values are shown in Fig. 11(a) and (b) respectively for different testing temperatures considered in present study. It could be observed from Fig. 11(b) that Barlat 1989 closely covers all the experimental points but Hill 1948 shows inability in capturing the whole yielding behavior of Inconel 625 especially in TD and ND directions. Banabic [64] stated that Hill 1948 has advantage that it has less number of constants which can be easily determined. Though, he also stated that Hill 1948 criteria does not have capability of yield stress prediction for uniaxial tensile testing which is a major drawback of this criteria. Thus, it could be concluded that prediction ability for yielding nature of Inconel 625 alloy is better with Barlat 1989 and could be used for numerical predictions in forming of sheet metals using FEA codes.

Forming behavior

Deep drawing

Deep drawing is an important forming process in mechanical industries. Excessive thinning is the main cause of concern in deep drawing process. It is always desired to have a deep drawn cup with least thickness variation along the cup. Several process parameters affect the thickness of drawn components of which effect of temperature, BHP and punch speed are considered in present case. Two different analysis viz., Target Performance Measure (TPM) and Noise Performance Measure (NPM) have been performed in MINITAB 17 software to get best set of process parameters for least thickness variation. NPM helps in identifying the set of process parameters which reduces the variation in the obtained experimental values and also helps in identifying how much affect it is having over the mean value of the desired output at a particular set of setting. The signal to noise (S/N) ratio is considered for analysis of NPM. Signal to Noise ratio is the measure used in optimization of process parameter that compares the level of a desired signal (useful resource) to the level of noise (wastage). The S/N ratio can be said to be defined as the ratio of

useful resource to the wastage. In determining the best set of process parameters, a measure of robustness is used to identify control factors that reduce variability in a product or process by minimizing the effects of uncontrollable factors (noise factors). Control factors are those design and process parameters that can be controlled. Noise factors cannot be controlled during production or product use, but can be controlled during experimentation. The noise factors can be manipulated to force variability to occur and from the results, identify optimal control factor settings that make the process or product robust, or resistant to variation from the noise factors. Higher values of the signal-to-noise ratio (S/N) identify control factor settings that minimize the effects of the noise factors. Mean responses are often considered in TPM analysis. Mean responses are the average values of all the iterations (3 in present case) for a set of experimental process parameters. The parameters which govern the NPM are known as variability process parameters while the parameters which govern the TPM are known as target process parameters. The average experimental thickness for different set of process parameters are reported in Table 9.

Analysis of Variance (ANOVA) is a statistical tool used to compare performance of each selected process parameter. It also gives quantitative comparison i.e. percentage contribution of each process parameter which helps in selecting the most influencing parameter towards the average thickness of drawn cup. The ANOVA table according to TPM analysis is represented in Table 8. In analysis of TPM, temperature or warm forming condition is having maximum contribution towards thickness distribution followed by BHP and punch speed for Inconel 625 alloy. It has been observed in all the cases that minimum and maximum thickness are obtained on punch corner region and at the flange region i.e. at the upper portion of the cup respectively. In order to find the relation between each parameter chosen for study and the response obtained is statistically significant, the Fisher value (F-value) and Probability value (p value) are obtained as shown in Table 10. The significance level chosen for p value analysis is 0.05 (5%). The parameter having p value less than the significance level chosen for study i.e. 0.05 is more statistically influencing the study. In present work temperature

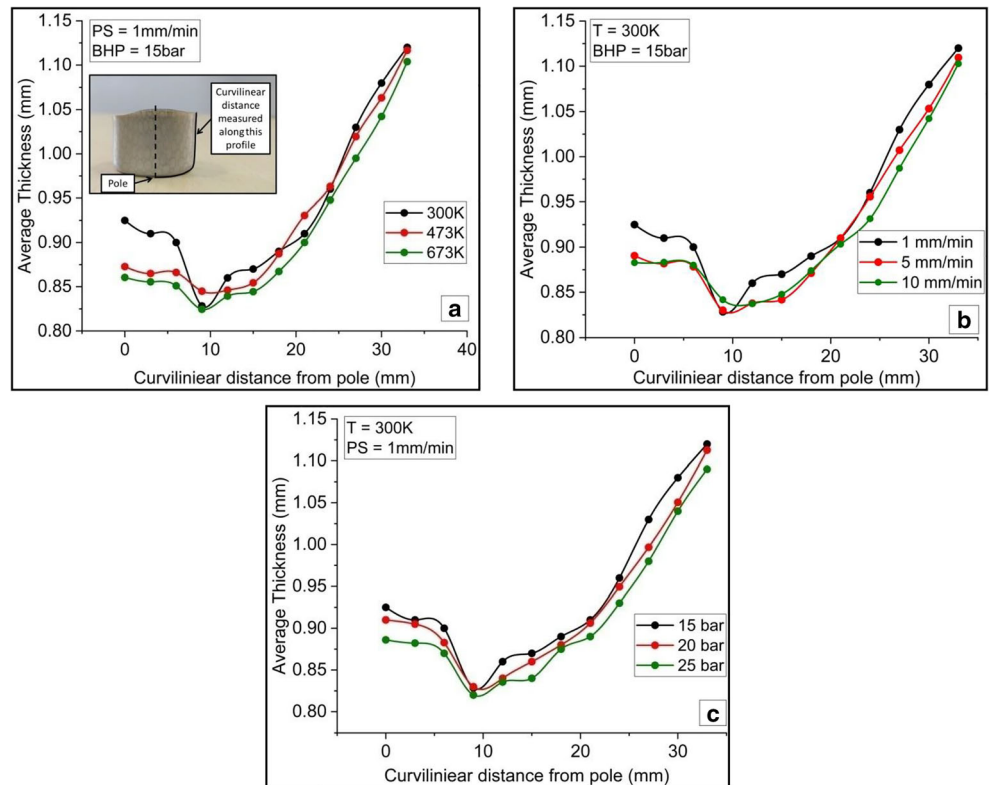
Table 11 Levels for different process parameters

Level Parameter	Level 1	Level 2	Level 3
Temperature	300 K	473 K	673 K
Punch Speed	1 mm/min	5 mm/min	10 mm/min
BHP	15 bar	20 bar	25 bar

Table 12 Response table for TPM

	Temperature	BHP	Punch Speed
Level 1	0.9340	0.9192	0.9238
Level 2	0.9284	0.9336	0.9271
Level 3	0.9152	0.9248	0.9269
Delta	0.0188	0.0145	0.0033
Rank	1	2	3

Fig. 12 Representative variation of average thickness for different (a) temperature, (b) punch speed and (c) BHP



(0.009) and BHP (0.052) are having more significant influence over thickness distribution than the punch speed (0.81). Also, the parameter having higher F-value as temperature in present case is considered have more influence over desired output i.e. least thickness distribution.

Different levels of process parameters considered in present work are defined in Table 11 with 3 different levels. The response table for TPM process is reported in Table 12. It could be clearly observed from the rank obtained for the process parameters in response table that temperature is the most influencing parameter towards thickness distribution followed by BHP and punch speed. The similar trend for process parameters was observed earlier from ANOVA analysis of TPM.

Representative variation of average thickness with curvilinear distance from pole of drawn cup has been reported in Fig. 12(a), (b) and (c) for temperature, punch speed and BHP respectively. The constant thickness has been observed along the base of the cup. Minimum thickness has been reported near the area of contact with punch nose. The thickness then gradually increases along the wall from bottom to top of cup. Variation in thickness is observed more in case of elevated temperature than that at 300 K. The material becomes soft at elevated temperature and hence the resistance to deformation decreases. It was also observed in section 3.1 of material properties determination that ductility of material increases at elevated temperature which facilitate easy and uniform drawing

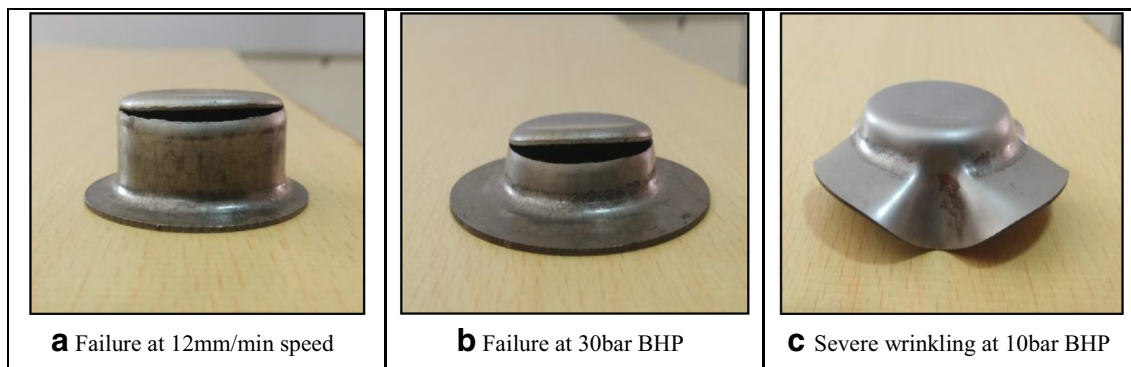


Fig. 13 Failure specimens during fixing of process parameters

of cups. The punch speed is believed to have least effect over thickness variation. However, at very high speed the chances of failure also increase in absence of sufficient lubrication as the material do not get sufficient time for forming as shown in Fig. 13(a). BHP also has significant effect over thickness distribution of cup. At higher BHP more thinning along the punch nose radius has been observed as it creates more hindrance in easy flow of material and also results in increased friction for contacts between blank, punch and die which ultimately results in failure in terms of fractured cup as shown in Fig. 13(b). Thus, for uniformity in thickness of deep drawn cup higher temperature and lower BHP are always preferred. But very low BHP also leads to undesired effect in terms of severe wrinkling as shown in Fig. 13(c). It is always advisable to have most optimum settings obtained from rigorous experimental analysis to get best quality cup from deep drawing process with uniform thickness.

For NPM, ANOVA analysis is shown in Table 13 and it has been observed that temperature and BHP are having effective contribution towards maximizing the S/N ratio which is the desired output. Based upon the delta value in response table for NPM as shown in Table 14, the ranks have been allotted to the parameters contributing in increasing the S/N ratio. The temperature (53.02% contribution) is having maximum influence followed by BHP (23.10% contribution) and punch speed (8.68% contribution) in case of NPM. NPM analysis is done to identify the set process parameters which help in reducing the variation in output response. S/N ratios are calculated on the basis of nominal is better setting in MINITAB 17 software as the objective is to bring uniformity in thickness distribution [16]. The S/N ratios are calculated based upon following Eq.16–18.

$$s/N = 10 \times \log_{10} \left(\frac{\bar{y}^2}{s^2} \right) \tag{16}$$

$$s^2 = \frac{\sum_{i=1}^n (y_i - \bar{y})^2}{(n-1)} \tag{17}$$

$$\bar{y} = \frac{\sum_{i=1}^n y_i}{n} \tag{18}$$

where, n is the total number of iterations and y_i is the thickness at i^{th} iteration. S/N ratio have been calculated for each set of

Table 13 ANOVA for S/N ratio

Source	DF	Seq. SS	F-Value	P Value	% Contribution
Temperature	2	43.08	3.73	0.048	53.02
BHP	2	18.77	1.32	0.095	23.10
Punch Speed	2	07.06	0.29	0.495	08.68
Residual Error	20	12.34	–	–	15.18
Total	26	81.25	–	–	100

Table 14 Response table for S/N ratio

	Temperature	BHP	Punch Speed
Level 1	37.13	36.68	37.13
Level 2	39.41	38.72	38.78
Level 3	36.47	37.57	37.07
Delta	2.94	2.04	1.72
Rank	1	2	3

experiment and shown in Table 9. Experiment 14 (temperature = 473 K, BHP = 20 bar and punch speed = 5 mm/min) is having highest S/N ratio i.e. 48.6884 and hence this setting could be considered to be optimal for performing deep drawing of Inconel 625 alloy in present case but further a confirmation test is required to be performed.

Different process parameters have been selected for confirmation test to bring the uniformity in thickness distribution on the basis of their % contribution over it. Different parameters considered are shown in Table 15 on the basis of their % contribution over desired output for NPM and TPM analysis. The process parameters are considered to be pooled if they are having less than 10% contribution over thickness distribution. If process parameters in case of both NPM and TPM were pooled, then it is considered that they are not having any significant contribution over output and the measure having more contribution percent is considered for analysis. But, if neither NPM nor TPM were pooled then that level of process parameter is considered which is having more significant contribution over output. If either NPM or TPM is pooled then the one which is not pooled, is considered for analysis. Optimum level of setting selected for each process parameter is shown in Table 16. These levels of process parameters have been selected on the basis of highest values obtained corresponding to that process parameter in response tables of TPM and NPM.

The optimum set of process parameters are Temperature (473 K), Punch Speed (5 mm/min) and BHP (20 bar) for uniformity in thickness distribution. No further confirmation testing of obtained optimum process parameters is required as experiment has already been performed (experiment 14) using these settings and average thickness obtained was 0.929 mm.

Table 15 Parameters considered for analysis

Process Parameter	TPM		NPM		Effect of factor
	% Contribution	Pooled	% Contribution	Pooled	
Temperature	49.80	No	53.02	No	Both
BHP	28.44	No	23.10	No	Both
Punch Speed	10.68	No	08.68	Yes	TPM

Table 16 Selected settings for each process parameter

Process Parameter	TPM		NPM		Selected Level	Actual Value
	Level	% contribution	Level	% contribution		
Temperature	1	49.80	2	53.02	2	473 K
BHP	2	28.44	2	23.10	2	20 bar
Punch Speed	2	10.68	2	08.68	2	5 mm/min

Stretch forming

All the experimental stretch formed specimens at different temperatures are shown in Fig. 14. Temperature as a process parameter has very significant effect over forming of metal. The deformed ellipse on stretched specimens have been used for finding true major and minor strains which in turn helped in plotting the FLD as shown in representative diagram at 300 K and 673 K in Fig. 15. The safe, necked and fractured ellipses are marked with different patterns in order to segregate the regions. All the measures of major and minor strain were taken on stereo microscope with least count of 0.1 μm. At all temperatures and designs the material failed without any substantial hint of necking in case of specimens lying in the tension-tension region specifically at 300 K. As a result very less number of necked points have been observed at RT. At elevated temperature, the material becomes soft and as a result the more necking has been observed. The fracture strains are marked by Fracture Curve (FC) and these lie above safe strain points. The representative FLD curve has been drawn at 300 K and 673 K by considering the ellipses with maximum safe strain and is shown in Fig. 15. Design 1, 2 and 3 lie in Tension-Tension region while design 4 and 5 lie in Tension-Compression region along different strain paths (α). Strains paths are calculated using Eq. 19. The material always posses

a limiting strain (minimum) near the region of plane strain in FLD which is also the intersection of FLD with the true major strain axis and is designated as FLD₀. This point defines the formability of material. With increase in temperature, the formability of material also increases and hence FLD₀ shifts upwards on true major strain axis. For 300 K the FLD₀ has been observed at 0.33 true major strain which is very much comparable to the previous work done by Roamer et al. on Inconel 625 [34]. The FLD₀ at 473 K and 673 K have been observed at 0.4 and 0.45 true major strain respectively.

$$\alpha = \frac{\text{True minor strain}}{\text{True major strain}} \tag{19}$$

The sub-sized hemispherical punch (diameter = 50 mm) is used in present study instead of standard punch (diameter = 101.4 mm) as suggested by Hecker [42]. Thus, the bending strain effect have been observed over outer surface of blank while stretch forming by smaller size punch. It is necessary to consider this effect of punch curvature on stretching limits as specimens have been deformed into a convex shape. This strain gradient effect along thickness of a sheet on strain measurement has been reported in the literature and the position of FLD is highly dependent on it [66]. Specifically, the punch curvature (1/R) has been found to be directly proportional to

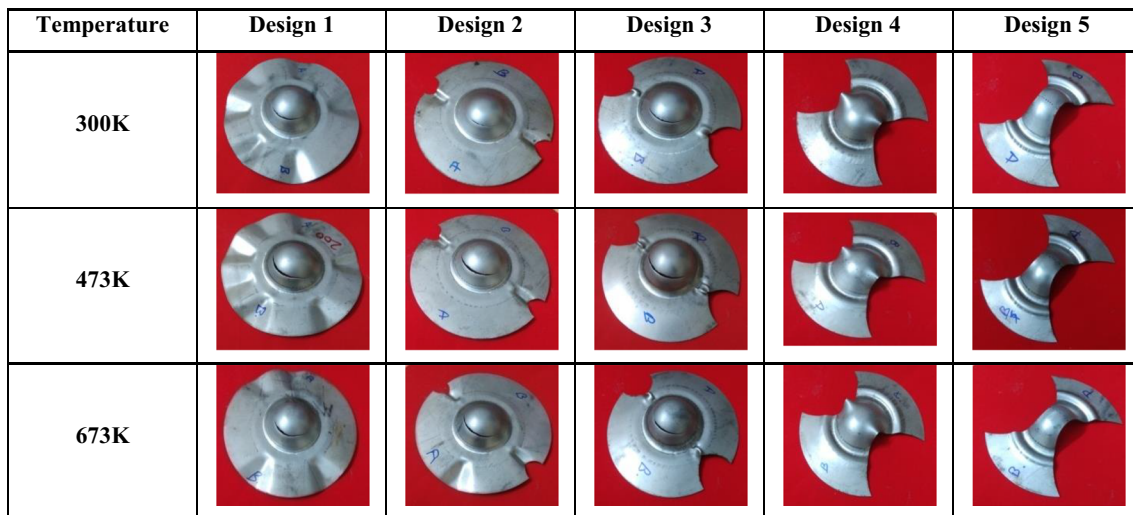
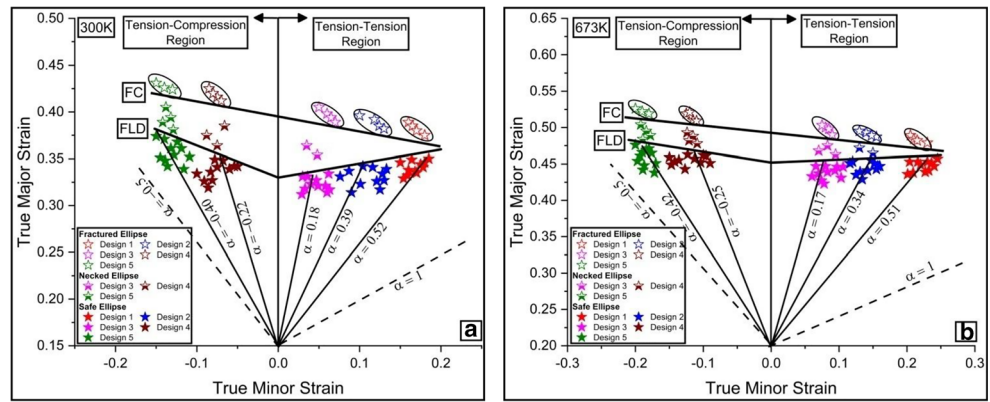


Fig. 14 Stretch formed specimens at different testing temperatures

Fig. 15 Representative FLD and FC at (a) 300 K and (b) 673 K



limiting strains at constant sheet thickness [67]. Bending strain is mathematical expressed by Eq.20.

$$\epsilon_{\text{bending}} = \ln\left(1 + \frac{t_f}{2R_n}\right), \text{ where } t_f = t_0 - \exp(-\epsilon_{1m} - \epsilon_{2m}) \quad (20)$$

where, ϵ_{1m} and ϵ_{2m} represent measured true major and minor surface strains, t_0 = initial thickness, t_f = instantaneous thickness (onset of necking) and R_n = radius of curvature of the middle surface of the sheet. Thus, for accurate prediction of limiting strain values, it is an essential to consider the effect of bending strain in the FLD prediction. The measured surface strain is a combination of stretching and bending strains. In order to measure correct limiting surface strains ($\epsilon_{1,2}$), induced bending strains have been deducted from measured true strains using Eq. 21.

$$\epsilon_{1,2} = \epsilon_{1m,2m} - \epsilon_{\text{bending}} \quad (21)$$

Limiting strains in FLD has been corrected by using Eq. (14) and (15). Figure 16 shows the corrected FLD and FC. It has been observed that the corrected FLD and FC shifted downwards by approximately 5–6% in all the strain regions at all test temperatures.

Strain distribution across the component produced by stretch forming process is very much important phenomena in manufacturing industries. To get an idea for strain distribution across the stretched part, the variation of surface strain with respect to the curvilinear distance from pole are examined for different testing temperatures in present study and design 1 and 5 samples as shown in Fig.17(a) and (b) respectively. By the method of circular grid analysis, the strain measurement was done along the rolling direction of sheet. The pole is considered to be tip of hemispherical cup and curvilinear distance from it is considered for analysis.

In case of design 5 sample major strain was found to increase till 12 mm curvilinear distance for 300 K and 473 K temperature and 15 mm curvilinear distance for 673 K. Further on increasing the curvilinear distance, the gradual decrease in strain was observed for major strain. It was also observed that with increase in temperature, highest major strain increased and lowest minor strain decreased as the drawability of metal also increased with temperature. The positive value of major strain and negative value of minor strain was observed for all the temperatures across the whole range of distance which shows that the specimen is drawn laterally [68]. In case of design 1 specimens, both the minor and major strain moved to first quadrant and hence it could be

Fig. 16 Experimental and corrected (a) FLD and (b) FC at different test temperatures

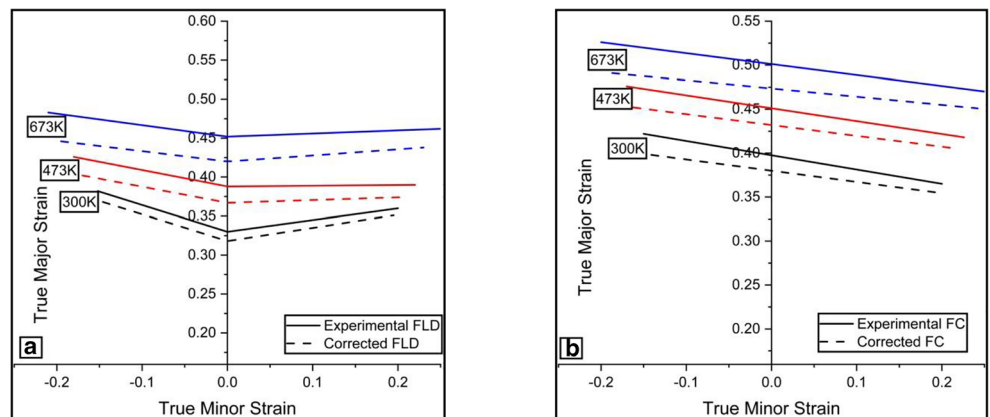
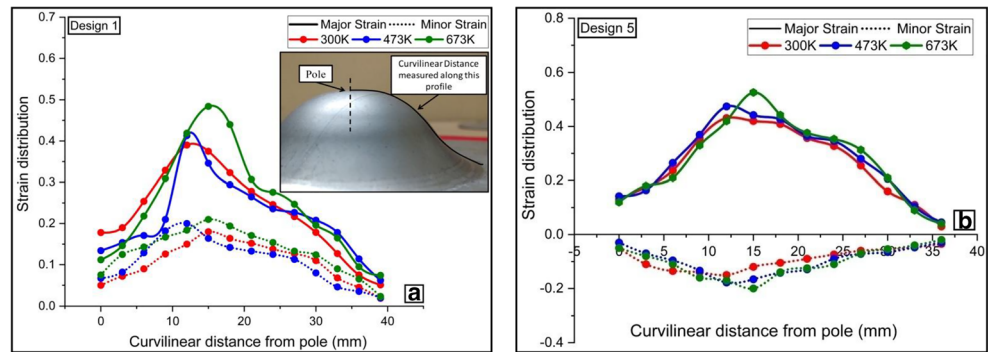


Fig. 17 Surface strain plots for (a) Design 1 and (b) Design 5



said that tension-tension nature will be displayed by this specimen. This further confirms that mode of stretching observed is biaxial. The highest major strain was observed at approximately 15 mm distance from pole for 673 K and 12 mm for 300 K and 473 K. Similar trend was observed for minor strain as well for 473 K and 673 K curves but maximum of minor strain at 300 K was observed at 15 mm distance.

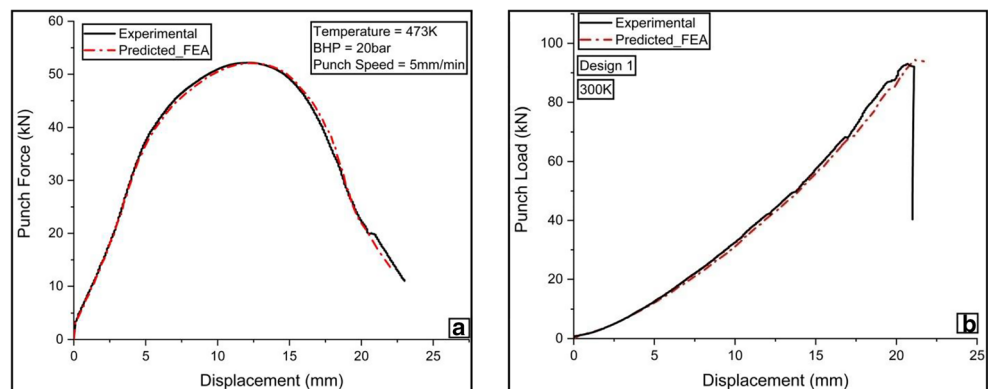
Finite element analysis

Deep drawing process with flat bottom punch have been numerically simulated in ABAQUS 6.13 software. The CAD model has been prepared in Solidworks-14 software. In section 3.2.1 of constitutive modeling it was found that the m-A model is best suited for prediction of flow stress for Inconel 625 alloy. It was also found in section 3.2.2 of yield criterion that Barlat 1989 best suits the anisotropic yielding behavior of material. Hence, to have the effect of constitutive models along with yield criterion UMAT subroutine has been built and incorporated with numerical solver package, ABAQUS 6.13 for obtaining comparable desired outputs from stretch forming and deep drawing process. The CAD file of deep drawing process consist of 4 different components viz., blank holder plate, die, punch and blank. The blank holder plate, die and punch have been assigned discrete rigid property as no particular

results and observations need to be done over them. The mesh element type used for these components in ABAQUS solver is R3D4. All the observations need to be done over blank and so it has been assigned as deformable body property and C3D8R solid elements have been used for it. The representative punch force vs. displacement for deep drawing and stretching process has been compared in Fig. 18. The suitability of applied constitutive model and anisotropic yield criteria has been proved by comparing the numerically predicted results with the experimental results.

The whole deep drawing setup is symmetric, therefore only one-fourth (quarter) of the geometry is considered for analysis so as to decrease the computational time. The obtained results are then mirrored along consecutive planes for obtaining full cup. Study of mesh convergence has also been carried out so to have final optimum size of elements. The rigid elements were considered over blank holder plate, punch and die, therefore coarse mesh of size approximately 5 × 5 mm has been assigned to them. But blank is a critical deformable component, therefore rigorous mesh convergence analysis [69] has been carried out and elements of size 1.5 × 1.5 mm has been finalized on the basis computational time and relative error compared between obtained numerical and experimental average thickness for most optimal setting obtained from section 3.3.1 of deep drawing analysis in present work. Further same

Fig. 18 Representative Punch force vs. Displacement graph for (a) Deep Drawing and (b) Stretching process



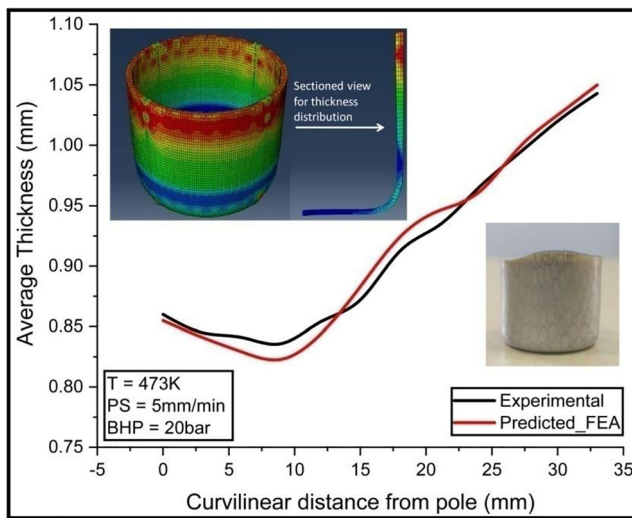


Fig. 19 Representative comparison of thickness distribution for FEA and experimental deep drawn cup

mesh size has been used for all simulations with different set of parameter settings. Total number of mesh elements over blank of 58 mm diameter and 1 mm thickness were 12,896. Material properties calculated and shown in section 3.1 are used as an input for performing deep drawing simulations. The friction coefficient has been considered as 0.15 between all contacts for FEA study.

The representative comparison of predicted and experimental thickness obtained at setting ($T = 473$ K, $PS = 5$ mm/min and $BHP = 20$ bar) is shown in Fig. 19. The vertical drawn height of cup has been evaluated by measuring the distance between lowest to the uppermost node of the cup. Uniformity in thickness of drawn cup is the main concern and hence relative error has been evaluated between experimental and numerically obtained results in order to validate the numerical analysis. The average error percent observed in case thickness distribution and drawn height was 3.83% and 4.06% respectively which are well within the 5% of acceptance level. Thus, m-A constitutive model along with Barlat 1989 yield criteria are best suited for performing the FEA simulation of deep drawing process for Inconel 625 alloy.

Full geometry analysis of stretch forming process has been carried out in ABAQUS 6.13 solver. Mesh convergence study

has been carried out and fixed elements of size 5×5 mm has been considered over blank holder plate, punch and die. As all results are desired over blank, therefore mesh sensitivity analysis has been carried out for all 5 design of specimens. The mesh element type used over blank is C3D8R solid elements. The final mesh size, number of elements and computational time are shown in Table 17. Computational time and error of LDH between experimental and FEA study are used as a measure to finalize the mesh size and further it is used in performing FEA studies at all considered temperatures. Material properties calculated in section 3.1 are used as an input for performing stretch forming simulations and the friction coefficient has been considered as 0.15 between all contacts for FEA study.

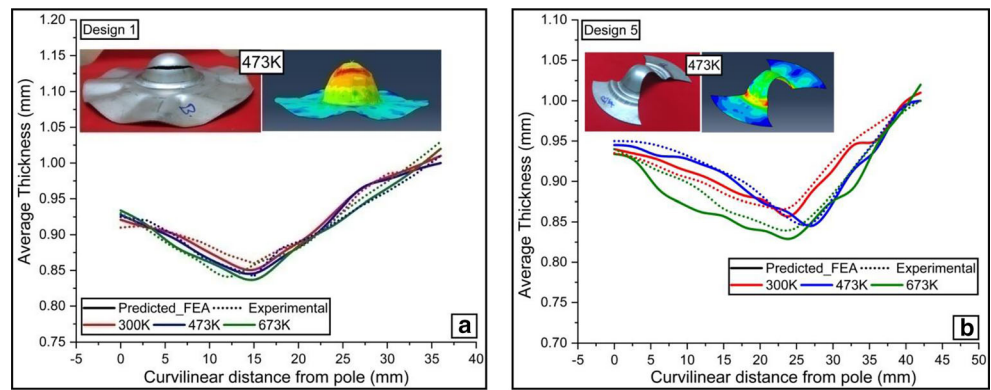
Representative average thickness distribution for Design 1 and 5 has been reported by measuring each specimen 3 times in Fig. 20. It was observed that the thickness of cup remains almost constant initially i.e. near the pole of specimen and then it started decreasing and minimum thickness was observed at place where necking and fracture occur. The thickness then further increased gradually till the flange portion of specimen. Thickness almost equal to the sheet thickness was observed on the flat flange part of specimen. Similar nature of plot was observed for different designs at various considered temperatures in present study. The thickness was observed to decrease with increase in temperature as the material become soft and hence the drawability also increases which resulted in long but thin necking portion. FEA results also show similar nature of curve as in case of experimental results. For design 1 samples, lowest thickness has been observed at approximately 15 mm pole distance for 300 K and 473 K in case of both FEA and experimental results. At 673 K, least experimental thickness was observed at 12 mm distance from pole but in case of FEA it is at 15 mm distance. For design 5, minimum thickness was observed at approximately 24 mm distance for 300 K and 673 K while at 473 K it occurred at approximately 27 mm distance from pole of sample.

LDH is an important phenomena in determining the formability of material. Experimental and predicted LDH at different temperature is shown in Fig. 21. The LDH seem to increase with increase in temperature as the material becomes soft and hence the formability also increases. The relative error between predicted and experimental LDH at various

Table 17 Mesh sensitivity analysis for Stretch forming

	Element Size (mm)	Total elements on blank	Computational Time (s)
Design 1	1.5×1.5	1209	3857
Design 2	1×1	1463	4761
Design 3	1×1	1362	4423
Design 4	1×1	1258	4008
Design 5	0.5×0.5	1347	4264

Fig. 20 Representative predicted and experimental thickness observed for (a) Design 1 and (b) Design 5



testing temperatures for all designs was well within the 5% of acceptance level. Thus, m-A constitutive model and Barlat 1989 yield criteria can be used as a combination for performing stretch forming FEA studies of Inconel 625 alloy.

Conclusions

The material modeling and forming behavior have been discussed in present work over Inconel 625 alloy. Some of the important conclusions are listed below.

- Flow stress behavior was found to be significantly affected by process parameters such as temperature and deformation rate of material. With increment in testing temperature from 300 K to 673 K, the yield and ultimate stress decreased by approximately 25% and 17% respectively. DSA effect has also been observed for flow stress at 673 K.
- Four different constitutive models namely; modified Jhonson-Cook (m-JC), modified Zerilli-Armstrong (m-ZA), modified Arrhenius (m-A), Khan–Huang–Liang (KHL) model have been established based on experimental flow stress data. The m-A model best predicts the flow stress behavior as it is having best statistical parameters such as $R = 0.9721$, $\Delta = 5.2616\%$ and $\delta = 2.314\%$. Anisotropic yield criterion viz., Hill 1948 and Barlat

1989 have also been implemented and it was found that Barlat 1989 best predicts the yielding nature of Inconel 625 alloy.

- Forming behavior of Inconel 625 alloy is analyzed based on circular deep drawing and stretch forming process. Variation in thickness along the wall in deep drawing process is the major cause of concern and hence thorough analysis has been conducted by varying different considered process parameters. Using TPM and NPM methods it has been found that best quality cups have been drawn at 473 K using 20 Bar pressure and 5 mm/min as drawing speed. The temperature was found to be most influential parameter over thickness distribution in deep drawing process having total contribution of 49.8% followed by BHP, 28.44% and punch speed 10.68%. The FLDs and FCs are plotted at different temperatures and it was found that temperature change has significant effect on limiting strain of the material.
- UMAT subroutine with m-A model and Barlat 1989 criteria have been used for FEA of deep drawing and stretch forming process. The average error between FEA and experimental results of deep drawing process was found to be 3.83% for thickness distribution and 4.06% for drawn height. The relative error between predicted and experimental LDH and thickness distribution at various testing temperatures for all designs was found to be well within the 5% of acceptance level in case of stretch forming.

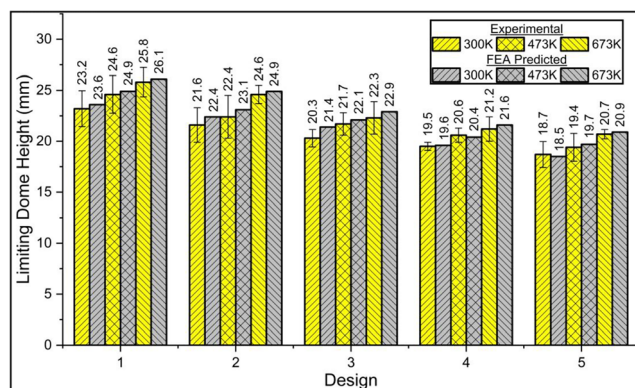


Fig. 21 Experimental and Predicted LDH at different temperature

Further work involves plotting of stress based FLD and theoretical prediction of strain based FLD using M-K model.

Acknowledgements Authors pay their high regards towards Science and Engineering Research Board (SERB), Government of India for funding the project (file number - ECR/2016/001402). Authors are also thankful to BITS-Pilani, Hyderabad Campus for providing the UTM facility in Central Analytical Lab (CAL).

Compliance with ethical standards

Conflict of interests The authors declare that they have no conflict of interest.

References

- Kotkunde N, Badrish A, Morchhale A, Takalkar P, Singh SK (2019) Warm deep drawing behavior of Inconel 625 alloy using constitutive modelling and anisotropic yield criteria. *Int J Mater Form*. <https://doi.org/10.1007/s12289-019-01505-3>
- Thakur DG, Ramamoorthy B, Vijayaraghavan L (2009) Machinability investigation of Inconel 718 in high-speed turning. *Int J Adv Manuf Technol* 45(5-6):421. <https://doi.org/10.1007/s00170-009-1987-x>
- Lin YC, Wen D-X, Deng J et al (2014) Constitutive models for high-temperature flow behaviors of a Ni-based superalloy. *Mater Des* 59:115–123. <https://doi.org/10.1016/j.matdes.2014.02.041>
- Wen D-X, Lin YC, Li H-B et al (2014) Hot deformation behavior and processing map of a typical Ni-based superalloy. *Mater Sci Eng A* 591:183–192. <https://doi.org/10.1016/j.msea.2013.09.049>
- Lin YC, Li K-K, Li H-B et al (2015) New constitutive model for high-temperature deformation behavior of inconel 718 superalloy. *Mater Des* 74:108–118. <https://doi.org/10.1016/j.matdes.2015.03.001>
- Grzesik W, Nieslony P, Laskowski P (2017) Determination of material constitutive Laws for Inconel 718 Superalloy under different strain rates and working temperatures. *J of Materi Eng and Perform* 26(12):5705–5714. <https://doi.org/10.1007/s11665-017-3017-8>
- Gujrati R, Gupta C, Jha JS et al (2019) Understanding activation energy of dynamic recrystallization in Inconel 718. *Mater Sci Eng A* 744:638–651. <https://doi.org/10.1016/j.msea.2018.12.008>
- Zhou Y, Chen X-M, Qin S (2019) A strain-compensated constitutive model for describing the hot compressive deformation behaviors of an aged Inconel 718 Superalloy. *High Temperature Materials and Processes* 38:436–443. <https://doi.org/10.1515/htmp-2018-0108>
- Lin YC, Chen X-M (2011) A critical review of experimental results and constitutive descriptions for metals and alloys in hot working. *Mater Des* 32:1733–1759. <https://doi.org/10.1016/j.matdes.2010.11.048>
- Liu D, Zhang X, Qin X, Ding Y (2017) High-temperature mechanical properties of Inconel-625: role of carbides and delta phase. *Mater Sci Technol* 33:1610–1617. <https://doi.org/10.1080/02670836.2017.1300365>
- Pandre S, Takalkar P, Morchhale A, Kotkunde N, Singh SK (2020) Prediction capability of anisotropic yielding behaviour for DP590 steel at elevated temperatures. *Advances in Materials and Processing Technologies*. <https://doi.org/10.1080/2374068X.2020.1728647>
- Prasad KS, Kamal T, Panda SK et al (2015) Finite element validation of forming limit diagram of IN-718 sheet metal. *Materials Today: Proceedings* 2:2037–2045. <https://doi.org/10.1016/j.matpr.2015.07.174>
- Kotkunde N, Deole AD, Gupta AK, Singh SK (2014) Experimental and numerical investigation of anisotropic yield criteria for warm deep drawing of Ti–6Al–4V alloy. *Mater Des* 63:336–344. <https://doi.org/10.1016/j.matdes.2014.06.017>
- Jeswiet J, Geiger M, Engel U et al (2008) Metal forming progress since 2000. *CIRP J Manuf Sci Technol* 1:2–17. <https://doi.org/10.1016/j.cirpj.2008.06.005>
- Yoon BB, Rao RS, Kikuchi N (1989) Sheet stretching: a theoretical-experimental comparison. *Int J Mech Sci* 31:579–590. [https://doi.org/10.1016/0020-7403\(89\)90065-9](https://doi.org/10.1016/0020-7403(89)90065-9)
- Kardan M, Parvizi A, Askari A (2018) Experimental and finite element results for optimization of punch force and thickness distribution in deep drawing process. *Arab J Sci Eng* 43(3):1165–1175. <https://doi.org/10.1007/s13369-017-2783-9>
- Savaş V, Seçgin Ö (2010) An experimental investigation of forming load and side-wall thickness obtained by a new deep drawing die. *Int J Mater Form* 3(3):209–213. <https://doi.org/10.1007/s12289-009-0672-9>
- Boissière R, Vacher P, Blandin JJ (2010) Influence of the punch geometry and sample size on the deep-drawing limits in expansion of an Aluminium alloy. *Int J Mater Form* 3(1):135–138. <https://doi.org/10.1007/s12289-010-0725-0>
- Morchhale A (2016) Design and finite element analysis of hydrostatic pressure testing machine used for ductile Iron pipes. *MER* 6: 23. <https://doi.org/10.5539/mer.v6n2p23>
- Venkateswarlu G, Davidson MJ, Tagore GRN (2010) Influence of process parameters on the cup drawing of aluminium 7075 sheet. *International journal of engineering, science and technology* 2:
- Ahmetoglu M, Broek TR, Kinzel G, Altan T (1995) Control of blank holder force to eliminate wrinkling and fracture in deep-drawing rectangular parts. *CIRP Ann* 44:247–250. [https://doi.org/10.1016/S0007-8506\(07\)62318-X](https://doi.org/10.1016/S0007-8506(07)62318-X)
- Wallmeier M, Linvill E, Hauptmann M et al (2015) Explicit FEM analysis of the deep drawing of paperboard. *Mech Mater* 89:202–215. <https://doi.org/10.1016/j.mechmat.2015.06.014>
- Prasad KS, Panda SK, Kar SK et al (2018) Prediction of fracture and deep drawing behavior of solution treated Inconel-718 sheets: numerical modeling and experimental validation. *Mater Sci Eng A* 733:393–407. <https://doi.org/10.1016/j.msea.2018.07.007>
- Padmanabhan R, Oliveira MC, Alves JL, Menezes LF (2009) Stochastic analysis of a deep drawing process using finite element simulations. *Int J Mater Form* 2(1):347. <https://doi.org/10.1007/s12289-009-0565-y>
- Choudhury IA, Ghomi V (2014) Springback reduction of aluminum sheet in V-bending dies. *Proc Inst Mech Eng B J Eng Manuf* 228:917–926. <https://doi.org/10.1177/0954405413514225>
- Badrish A, Morchhale A, Kotkunde N, Singh SK (2020) Parameter Optimization in the Thermo-mechanical V-Bending Process to Minimize Springback of Inconel 625 Alloy. *Arab J Sci Eng*. <https://doi.org/10.1007/s13369-020-04395-9>
- Djavanroodi F, Derogar A (2010) Experimental and numerical evaluation of forming limit diagram for Ti6Al4V titanium and Al6061-T6 aluminum alloys sheets. *Mater Des* 31:4866–4875. <https://doi.org/10.1016/j.matdes.2010.05.030>
- He M, Li F, Wang Z (2011) Forming limit stress diagram prediction of aluminum alloy 5052 based on GTN model parameters determined by in situ tensile test. *Chin J Aeronaut* 24:378–386. [https://doi.org/10.1016/S1000-9361\(11\)60045-9](https://doi.org/10.1016/S1000-9361(11)60045-9)
- Bleck W, Deng Z, Papamantellos K, Gusek CO (1998) A comparative study of the forming-limit diagram models for sheet steels. *J Mater Process Technol* 83:223–230. [https://doi.org/10.1016/S0924-0136\(98\)00066-1](https://doi.org/10.1016/S0924-0136(98)00066-1)
- Panich S, Barlat F, Uthaisangsuk V et al (2013) Experimental and theoretical formability analysis using strain and stress based forming limit diagram for advanced high strength steels. *Mater Des* 51:756–766. <https://doi.org/10.1016/j.matdes.2013.04.080>
- Badr OM, Rolfe B, Hodgson P, Weiss M (2015) Forming of high strength titanium sheet at room temperature. *Mater Des* 66:618–626. <https://doi.org/10.1016/j.matdes.2014.03.008>
- Bong HJ, Barlat F, Lee M-G, Ahn DC (2012) The forming limit diagram of ferritic stainless steel sheets: experiments and modeling. *Int J Mech Sci* 64:1–10. <https://doi.org/10.1016/j.jimecs.2012.08.009>
- Shu J, Bi H, Li X, Xu Z (2012) Effect of Ti addition on forming limit diagrams of Nb-bearing ferritic stainless steel. *J Mater Process Technol* 212:59–65. <https://doi.org/10.1016/j.jmatprotec.2011.08.004>
- Roamer P, Van Tyne CJ, Matlock DK, et al (1997) Room temperature formability of alloys 625LCF, 718 and 718SPF. In: *Superalloys 718, 625, 706 and various derivatives* (1997). TMS, pp 315–329

35. Han HN, Kim K-H (2003) A ductile fracture criterion in sheet metal forming process. *J Mater Process Technol* 142:231–238. [https://doi.org/10.1016/S0924-0136\(03\)00587-9](https://doi.org/10.1016/S0924-0136(03)00587-9)
36. Jain M, Allin J, Lloyd DJ (1999) Fracture limit prediction using ductile fracture criteria for forming of an automotive aluminum sheet. *Int J Mech Sci* 41:1273–1288. [https://doi.org/10.1016/S0020-7403\(98\)00070-8](https://doi.org/10.1016/S0020-7403(98)00070-8)
37. Jeswiet J, Micari F, Hirt G et al (2005) Asymmetric single point incremental forming of sheet metal. *CIRP Ann* 54:88–114. [https://doi.org/10.1016/S0007-8506\(07\)60021-3](https://doi.org/10.1016/S0007-8506(07)60021-3)
38. Embury JD, Duncan JL (1981) Formability maps. *Annu Rev Mater Sci* 11:505–521. <https://doi.org/10.1146/annurev.ms.11.080181.002445>
39. Takuda H, Mori K, Takakura N, Yamaguchi K (2000) Finite element analysis of limit strains in biaxial stretching of sheet metals allowing for ductile fracture. *Int J Mech Sci* 42:785–798. [https://doi.org/10.1016/S0020-7403\(99\)00018-1](https://doi.org/10.1016/S0020-7403(99)00018-1)
40. Prasad YVRK, Rao KP, Sasidhara S (2015) Hot working guide: a compendium of processing maps, second edition, first printing. ASM International, Materials Park, Ohio
41. E28 Committee Test Methods for Tension Testing of Metallic Materials. ASTM International
42. Hecker SS (1975) Simple technique for determining forming limit curves. *Sheet Metal Industries* 52:671–676
43. Dieter GE, Bacon DJ (1986) Mechanical metallurgy. McGraw-hill New York
44. Li D, Guo Q, Guo S et al (2011) The microstructure evolution and nucleation mechanisms of dynamic recrystallization in hot-deformed Inconel 625 superalloy. *Mater Des* 32:696–705. <https://doi.org/10.1016/j.matdes.2010.07.040>
45. Liu J, Cui Z, Li C (2008) Analysis of metal workability by integration of FEM and 3-D processing maps. *J Mater Process Technol* 205:497–505. <https://doi.org/10.1016/j.jmatprotec.2007.11.308>
46. Kuhlmann-Wilsdorf D (1989) Theory of plastic deformation: - properties of low energy dislocation structures. *Mater Sci Eng A* 113:1–41. [https://doi.org/10.1016/0921-5093\(89\)90290-6](https://doi.org/10.1016/0921-5093(89)90290-6)
47. Rodriguez P (1984) Serrated plastic flow. *Bull Mater Sci* 6:653–663. <https://doi.org/10.1007/BF02743993>
48. Lin YC, Yang H, Chen X-M, Chen D-D (2018) Influences of initial microstructures on Portevin-Le Chatelier effect and mechanical properties of a Ni–Fe–Cr–Base Superalloy. *Adv Eng Mater* 20:1800234. <https://doi.org/10.1002/adem.201800234>
49. Hussaini SM, Singh SK, Gupta AK (2014) Formability of austenitic stainless steel 316 sheet in dynamic strain aging regime. *Acta Metall Slovaca* 20:71–81. <https://doi.org/10.12776/ams.v20i1.187>
50. Pandre S, Kotkunde N, Takalkar P, Morchhale A, Sujith R, Singh SK (2019) Flow stress behavior, constitutive modeling, and microstructural characteristics of DP 590 steel at elevated temperatures. *J of Materi Eng and Perform* 28(12):7565–7581. <https://doi.org/10.1007/s11665-019-04497-y>
51. Robinson JM, Shaw MP (1994) Microstructural and mechanical influences on dynamic strain aging phenomena. *Int Mater Rev* 39:113–122. <https://doi.org/10.1179/imr.1994.39.3.113>
52. Hosford WF, Caddell RM (2007) Metal forming by William F. Hosford. In: Cambridge Core. /core/books/metal-forming/DFD3C93FFFCB89A29076C55B8A4E1831. Accessed 5 Nov 2019
53. Johnson GR, Cook WH, Johnson G, Cook WA constitutive model and data for materials subjected to large strains, high strain rates, and high temperatures
54. Khan AS, Zhang H, Takacs L (2000) Mechanical response and modeling of fully compacted nanocrystalline iron and copper. *Int J Plast* 16:1459–1476. [https://doi.org/10.1016/S0749-6419\(00\)00023-1](https://doi.org/10.1016/S0749-6419(00)00023-1)
55. Sellars CM, McTegart WJ (1966) On the mechanism of hot deformation. *Acta Metall* 14:1136–1138. [https://doi.org/10.1016/0001-6160\(66\)90207-0](https://doi.org/10.1016/0001-6160(66)90207-0)
56. Armstrong RW, Arnold W, Zerilli FJ (2009) Dislocation mechanics of copper and iron in high rate deformation tests. *J Appl Phys* 105:023511. <https://doi.org/10.1063/1.3067764>
57. Lin YC, Chen X-M (2010) A combined Johnson–Cook and Zerilli–Armstrong model for hot compressed typical high-strength alloy steel. *Comput Mater Sci* 49:628–633. <https://doi.org/10.1016/j.commatsci.2010.06.004>
58. Lin YC, Chen X-M, Liu G (2010) A modified Johnson–Cook model for tensile behaviors of typical high-strength alloy steel. *Mater Sci Eng A* 527:6980–6986. <https://doi.org/10.1016/j.msea.2010.07.061>
59. Samantaray D, Mandal S, Bhaduri AK (2009) A comparative study on Johnson Cook, modified Zerilli–Armstrong and Arrhenius-type constitutive models to predict elevated temperature flow behaviour in modified 9Cr–1Mo steel. *Comput Mater Sci* 47:568–576. <https://doi.org/10.1016/j.commatsci.2009.09.025>
60. Prasad KS, Gupta AK (2014) A constitutive description to predict high-temperature flow stress in austenitic stainless steel 316. *Procedia Mater Sci* 6:347–353. <https://doi.org/10.1016/j.mspro.2014.07.044>
61. Johnson GR, Cook WH (1985) Fracture characteristics of three metals subjected to various strains, strain rates, temperatures and pressures. *Eng Fract Mech* 21:31–48. [https://doi.org/10.1016/0013-7944\(85\)90052-9](https://doi.org/10.1016/0013-7944(85)90052-9)
62. Badrish AC, Morchhale A, Kotkunde N, Singh SK (2020) Experimental and finite element studies of springback using splitting test for Inconel 625 alloy. *Advances in Materials and Processing Technologies*. <https://doi.org/10.1080/2374068X.2020.1728644>
63. Hill R (1990) Constitutive modelling of orthotropic plasticity in sheet metals. *Journal of the Mechanics and Physics of Solids* 38:405–417. [https://doi.org/10.1016/0022-5096\(90\)90006-P](https://doi.org/10.1016/0022-5096(90)90006-P)
64. Banabic D (2010) Sheet metal forming processes: constitutive Modelling and numerical simulation. Springer-Verlag, Berlin Heidelberg
65. Barlat F, Brem JC, Yoon JW et al (2003) Plane stress yield function for aluminum alloy sheets—part 1: theory. *Int J Plast* 19:1297–1319. [https://doi.org/10.1016/S0749-6419\(02\)00019-0](https://doi.org/10.1016/S0749-6419(02)00019-0)
66. Sajun Prasad K, Panda SK, Kar SK, Sen M, Murty SVSN, Sharma SC (2017) Microstructures, forming limit and failure analyses of Inconel 718 sheets for fabrication of aerospace components. *J of Materi Eng and Perform* 26(4):1513–1530. <https://doi.org/10.1007/s11665-017-2547-4>
67. Charpentier PL (1975) Influence of punch curvature on the stretching limits of sheet steel. *Metall Trans A* 6(8):1665–1669. <https://doi.org/10.1007/BF02641986>
68. Bandyopadhyay K, Basak S, Prasad KS et al (2019) Improved formability prediction by modeling evolution of anisotropy of steel sheets. *Int J Solids Struct* 156–157:263–280. <https://doi.org/10.1016/j.ijsolstr.2018.08.024>
69. Morchhale A (2017) Study of positioning and dimensional optimization of angled stiffeners using finite element analysis of above ground storage tank. *International Journal of Research in Mechanical Engineering* 5:10–19

Publisher's note Springer Nature remains neutral with regard to jurisdictional claims in published maps and institutional affiliations.